Available online at www.sciencedirect.com

ScienceDirect

Geochimica et Cosmochimica Acta 235 (2018) 55–75

Geochimica et Cosmochimica Acta

www.elsevier.com/locate/gca

The potential of near-entrance stalagmites as high-resolution terrestrial paleoclimate proxies: Application of isotope and trace-element geochemistry to seasonally-resolved chronology

Peter E. Carlson *, Nathaniel R. Miller, Jay L. Banner, Daniel O. Breecker, Richard C. Casteel

The University of Texas at Austin, Department of Geological Sciences, United States

Received 3 March 2018; accepted in revised form 30 April 2018; available online 5 June 2018

Abstract

Sub-annually resolved environmental proxies can be valuable archives of climate change, but they are rare in terrestrial settings, and it can be difficult to verify their annual nature. We suggest that speleothems that grow in well-ventilated zones of caves may preserve such high-resolution records. Near-entrance cave environments are characterized by year-round, near-atmospheric CO_2 concentrations and are significantly influenced by surface air temperature fluctuations, particularly in temperate latitudes. Previous monitoring studies of a well-ventilated, temperate-latitude cave (Westcave Preserve, central Texas) have documented seasonal variations in the oxygen isotope composition of calcite grown on glass substrates (with winter $\delta^{18}O$ maxima and summer $\delta^{18}O$ minima) as well as seasonal variations in drip water trace element compositions. Extending this work to a stalagmite (WC-3) from the same drip site, we find that stalagmite $\delta^{18}O$ variations are similar in magnitude to the seasonal $\delta^{18}O$ variations previously observed for calcite grown on glass substrates, that stalagmite [Mg] variations have a similar seasonal period with winter minima and summer maxima, and that geochemical variations follow stalagmite growth fabric as mm-scale couplets comprising thin, slow-growing, compact sparry calcite laminae (winters) and thicker, fast-growing, porous-elongate columnar calcite laminae (summers). We interpret a high-resolution (weekly to monthly) 52-year record of $\delta^{18}O$, Mg, Sr, and Ba in WC-3, and report new monthly measurements of drip water and associated calcite grown on glass substrates. We find drip water $\delta^{18}O$ and [Mg]/[Ca] are essentially invariant and that seasonal variations in WC-3 calcite $\delta^{18}O$ and Mg concentration agree well with predicted temperature-dependent fractionation between water and calcite. WC-3 calcite Sr and Ba also vary, but with higher and more variable frequencies compared to $\delta^{18}O$ and [Mg]. The annual nature of $\delta^{18}O$ and [Mg] cycles is supported by monitoring and ^{14}C bomb-peak chronology. We suggest that stalagmite $\delta^{18}O$ and [Mg] vary primarily in response to large seasonal temperature changes in this setting, allowing for unambiguous differentiation between summer and winter calcite growth. From such $\delta^{18}O$- and [Mg]- derived sub-annual chronologies, the timing of enrichments in other geochemical species that are less directly coupled to external cave temperature (e.g., calcite Sr and Ba) can be considered as proxies of other important processes such as water-rock interaction in the epikarst, precipitation events, or subsurface respiration rates. The potential for this kind of multi-proxy, seasonally-resolved dating may add near-entrance stalagmites to the list (ice cores, lake varves, tree rings) of high-resolution terrestrial proxies available for paleoclimate studies.

Keywords: Sub-annual chronology; Near-entrance speleothem; Trace elements; Oxygen isotopes

* Corresponding author.
E-mail address: petercarlson@utexas.edu (P.E. Carlson).

https://doi.org/10.1016/j.gca.2018.04.036
0016-7037/

1. INTRODUCTION

Paleoclimate reconstructions endeavor to interpret the nature and history of climate change over a range of scales in both time and space. The temporal resolution of paleoclimate reconstructions depends upon the precision and accuracy of available age control available from natural records. In this regard, proxies that reliably encode environmental seasonality are of particular value, potentially offering chronologies capable of sub-annual resolution. In terrestrial settings, the list of environmental proxies capable of recording seasonality is short, and these proxies are often limited in geographic occurrence or difficult to validate their annual nature. Karst systems span a wide latitudinal range, covering ~15% of Earth's ice-free land (Stevanović, 2018), however, and laminated speleothems from regions influenced by strong seasonal contrasts may also offer seasonally-resolved proxy records (Boch et al., 2011). Provided the age and annual timing of lamina development can be constrained, the derived lamina chronologies can facilitate a wide range of high-resolution studies (e.g., seasonality of rainfall, temperature, soil productivity, and water resource management, Wolter et al., 1999; Raich et al., 2002; Weiss et al., 2009; Dong et al., 2010; growth and retreat of glaciers, Rupper et al., 2009; geographic distribution of C_3 and C_4 plants, Schwartz et al., 2006; and refined U-series-based age models, Shen et al., 2013). Speleothems may also encode variations in and above the cave environment that are non-periodic or stochastic in nature. Coupled with annually-resolved chronologies, the nature of these variations can be compared to historical or instrumental meteorological records to evaluate potential controls and achieve a better understanding of karst system processes.

Some speleothems have been shown to record annual variations, including: laminations caused by seasonal variations in calcite growth (Genty, 1992, 1993; Baker et al., 1993; Railsback et al., 1994; Genty and Quinif, 1996; Genty et al., 1997; Johnson et al., 2006; Baker et al., 2008), laminations caused by seasonal deposition of organic matter or detrital material (e.g., Allison, 1926; Baker et al., 1993; Shopov et al., 1994; McGarry and Baker, 2000), and trace element concentrations following seasonal changes in drip water chemistry (Kuczumow et al., 2003; Treble et al., 2003; Borsato et al., 2007; Mattey et al., 2010). In general, speleothems are useful terrestrial paleoclimate indicators because of their long and continuous growth histories, their widespread geographic distribution, and the wide applicability of high-precision U-series geochronology for constraining high-temporal-resolution proxy records (Schwarcz, 1986; Gascoyne, 1992; Wang et al., 2001; McDermott, 2004). When present, regular annual variations in speleothem growth and geochemical composition provide inherent age constraints on the timing and duration of important karst processes, but visible laminations and geochemical cycles in a stalagmite may not be reliably annual in nature. Some stalagmite records that are otherwise annually-laminated often include some years recording no cycles or laminations, and some years recording multiple cycles or laminations (Treble et al., 2005; Baker et al., 2008). The annual nature of these signals must therefore be confirmed by other age-constraint methods, such as radiometric dates and known events observed in the stalagmite record (e.g., Smith et al., 2009; Nagra et al., 2017), by a comprehensive understanding of karst processes through cave monitoring (e.g., Frisia et al., 2000) or through stalagmite growth modeling (e.g., Genty et al., 2001a,b).

For the few speleothem studies that achieve annual or sub-annual resolution, high resolution variations in oxygen isotope composition ($\delta^{18}O$) and trace elements (especially Mg, Sr, and Ba) in the speleothem calcite are interpreted as markers of environmental change. Variations in oxygen isotope compositions are often attributed to annual variation in rainfall oxygen isotope composition (e.g., Treble et al., 2005; Johnson et al., 2006; Orland et al., 2015), and Mg variations are often interpreted as a proxy for seasonal variations of groundwater flux and its interactions with the host rock (e.g., Fairchild et al., 2001; Treble et al., 2003; Borsato et al., 2007; Orland et al., 2014; Rutlidge et al., 2014). Both oxygen isotope fractionation and Mg partitioning between water and calcite are temperature-dependent processes (Mucci, 1987; Rosenthal et al., 1997; Kim and O'Neil, 1997; Huang and Fairchild, 2001), but speleothems are typically selected from environmentally stable, deep cave settings, where cave-air temperatures remain near mean annual temperature year-round (Davies, 1953).

The entrances of caves often experience significantly more temperature variation than deep within the cave (Davies, 1953; Spötl et al., 2005). With notable exceptions (e.g., Allison, 1926; Railsback et al., 1994; Roberts et al., 1998; Johnson et al., 2006; Couchoud et al., 2009), however, sites near the entrances of caves are typically avoided for paleoclimate studies owing to concerns about the high variability of temperature, relative humidity, rates of CO_2 degassing and calcium carbonate growth, biological activity, and uncertainties about how these variations impact the geochemical composition of drip waters and speleothem calcium carbonate (Hendy, 1971; Goede et al., 1990; Gascoyne, 1992; Lauritzen and Lundberg, 1999; White, 2007). The large seasonal variations in temperature that occur near cave entrances, however, could be useful as seasonal chronometers if recorded in near-entrance stalagmites. In near-entrance settings, if the $\delta^{18}O$ value of drip water does not significantly vary at a seasonal scale, temperature could be a primary control on speleothem $\delta^{18}O$ variations. Similarly, if drip water [Mg]/[Ca] are relatively invariant on a seasonal scale in a near-entrance cave setting, temperature may be a primary control on speleothem Mg variations. While temperature estimates based on either speleothem oxygen isotope values or Mg concentrations are subject to significant potential error, near-entrance cave environments in temperate regions may see enough seasonal variation in temperature that these temperature-sensitive proxies may act as useful annual chronometers.

At Westcave Preserve, the site of the current study, Feng et al. (2014) found that the $\delta^{18}O$ values of calcite grown on glass substrates (substrate calcite, hereafter; collected monthly, $n = 16$, October 2009 to March 2011) systematically fluctuated over a 2–3‰ range, following seasonal cave air temperature variations, with $\delta^{18}O$ minima

corresponding to warmer months. They also found that comparable $\delta^{18}O$ cycles were preserved within the upper 6.7 mm of Westcave stalagmite WC-3. Because drip water $\delta^{18}O$ values were relatively invariant (± 0.16‰ VSMOW; 1σ) compared to local rainwater (± 2.19‰ VSMOW; 1σ) over this monitoring interval, Feng et al. (2014) concluded that $\delta^{18}O$ variation of WC-3 substrate calcite and stalagmite calcite is primarily controlled by seasonal temperature variations, via the temperature-sensitive calcite-water oxygen isotope fractionation factor, rather than changes in drip water oxygen isotope composition. Casteel and Banner (2015) assessed elemental compositions of drip water from six Westcave monitoring sites over the same 2009–2011 interval and found positive correlations between temperature and drip water [Sr]/[Ca] and [Ba]/[Ca] at nearly all monitoring sites, but not between temperature and drip water [Mg]/[Ca]. The same study found that substrate calcite growth rates were primarily controlled by seasonal surface air temperature fluctuations, with increased summer growth rates and decreased winter growth rates. The findings by Feng et al. (2014) and Casteel and Banner (2015) suggest that stalagmites growing in Westcave may respond to temperature seasonality via variable $\delta^{18}O$ compositions and select trace elements, and that age models capable of sub-annual resolution can be established from these stalagmites. Here, we test these hypotheses by performing high-spatial-resolution analysis of $\delta^{18}O$, as well as of trace elements (Mg, Sr, Ba), over the entire length of stalagmite WC-3. Previous efforts to establish a high-resolution chronology for WC-3 by U-series techniques proved problematic, indicating only that the stalagmite grew within the last century (Feng et al., 2014). Therefore, to test the derived $\delta^{18}O$ and trace element age models, we integrate constraints provided by complementary radiocarbon measurements from samples collected along the entire WC-3 growth axis. In this effort, we suggest that first order temperature seasonality can be resolved as an annual chronometer (e.g., winters can be unambiguously resolved from summers), but do not claim that paleotemperatures are precisely recorded.

2. HYDROGEOLOGIC SETTING

The near-entrance stalagmite studied in this report (WC-3) is from a small, shallow cave (Westcave), located on the Edwards Plateau, approximately 50 km west of Austin, TX (Fig. 1). Central Texas has a subtropical/subhumid to semi-arid climate (Larkin and Bomar, 1983). Annual rainfall (~900 mm) in this region is bimodally distributed, with peaks in spring and late fall (Larkin and Bomar, 1983). Temperatures vary seasonally over a ~15–16 °C range, between winter lows (5–17 °C) and summer highs (21–33 °C; Feng et al., 2014).

Well-studied cave systems of the Edwards Plateau karst system are mainly "deep" caves that experience small year-round temperature variations and ventilate seasonally, preferentially building up CO_2 when outside temperatures are warmer than cave air temperatures (Banner et al., 2007; Wong et al., 2011; James et al., 2015). The warm-season buildup of CO_2 in "deep" cave environments causes calcite precipitation to slow or cease entirely below active drip sites during summer months (Banner et al., 2007; Wong et al., 2011; James et al., 2015). In contrast, Westcave has two large entrances and a small volume; its opening area-to-volume ratio (~0.02 m^2/m^3) is 7-20x larger than typical of deep cave systems in the region (from cave entrance areas and volumes reported in Banner et al., 2007; Feng et al., 2012, 2014; Fig. 1; Cowan et al., 2013). As a result,

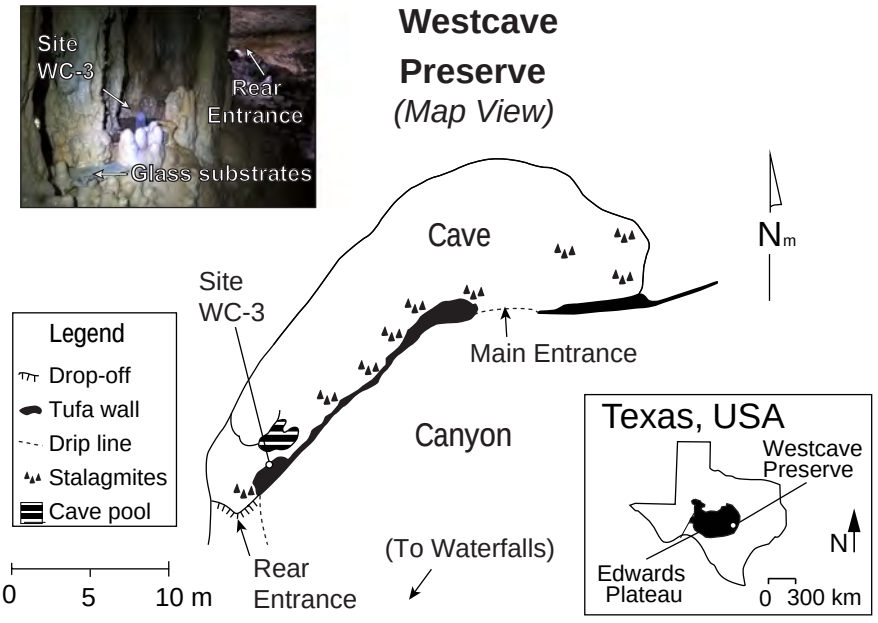

Fig. 1. Location map of Westcave Preserve within the Edwards Plateau of central Texas, and map of study site WC-3 near the rear entrance of Westcave (modified from Reddell and Smith, 1962; Feng et al., 2014). Photograph shows proximity of WC-3 to rear cave entrance as well as glass substrates used to measure calcite growth at drip water monitoring sites.

Westcave is perpetually well-ventilated, experiencing near-atmospheric CO_2 concentrations and near-surface air temperatures year-round (Feng et al., 2014). Because of these conditions, as well as relatively constant drip rates, speleothem growth rates in Westcave are continuous and higher year-round than in nearby deep caves, and increase during the summer rather than slow or cease (Casteel and Banner, 2015).

Westcave resides in the basal Cow Creek Limestone, above the contact with the underlying Hammett Shale, within a stream drainage (Heinz Branch Watershed) that contributes flow to the Pedernales River. Situated beneath a spring-fed waterfall, Westcave developed from combined erosion of basal Cow Creek strata and precipitation of tufa to partially enclose the cave. The waterfall and its plunge pool keep relative humidity of Westcave air higher than ambient air outside the cave (77–100%; Feng et al., 2014). Westcave speleothems grow from vadose water, transmitted through the overlying 20–25 m of Cow Creek Formation, entering the cave most obviously through short soda straws (2.5–15 cm; Feng et al., 2014). The near-entrance study site (WC-3), is located within 2 meters of the rear cave entrance (Fig. 1), and involves a single soda straw that feeds a ~10 cm stalagmite. Since collecting the stalagmite in June 2009, drip water and associated calcite, grown on glass substrates placed normal to and centered on the former stalagmite growth axis, have been collected at approximately monthly intervals (Feng et al., 2014; Casteel and Banner, 2015; this study).

3. METHODS

3.1. Stalagmite sampling

Geochemical sampling for laser ablation inductively-coupled plasma mass spectrometry (LA-ICP-MS) and micromilling for isotope-ratio mass spectrometry (IRMS) were performed on the surface of a 1-cm thick central-section slab of stalagmite WC-3. Intermittent porosity associated with a central depression required that sampling routes be laterally offset from the central growth axis, typically by <1 cm. A high-resolution digital color scan (Fig. 2) of the slab surface was used to identify optimal sampling routes positioned as close to and parallel to the central growth axis as possible, while avoiding large pores and areas previously sampled for U-series dating. Less-destructive LA-ICP-MS was performed first. Subsequent micromill sampling tracks typically overlaid, or were offset within 2 mm of laser traverses. Follow-up digital scans were used to precisely register LA-ICP-MS and micromill sampling positions on the primary reference slab image. To facilitate correlations between LA-ICP-MS transects and IRMS sample tracks, we digitized 46 growth-layer surfaces, hereafter termed "lamina datums" or LDs, that could be confidently traced laterally through both sampling tracks (Fig. 2, see insets A–C for detail). Although additional LDs could have been mapped, the 46 digitized LDs on average provide a stratigraphic control point approximately every 2 mm throughout the extent of WC-3. Large-format thin-sections, made from the opposing face of the stalagmite slab surface, shown in Fig. 2, were used along with the digital reference scan to characterize the petrography of WC-3 growth laminae (see electronic annex).

For LA-ICP-MS analysis, complete stratigraphic coverage required two laterally-offset sampling routes. Each route was analyzed in stratigraphic order, mainly as contiguous 1-cm transects, replicated *in situ* to evaluate sample and analytical reproducibility, using a 50×150 μm (H × W) rectangular aperture. The main "right" traverse begins at the central base of stalagmite WC-3 and ends at the top of the stalagmite to the right of the central high-porosity zone (Fig. 2). Maintaining growth-axis-parallel sampling required a 17° counterclockwise rotational shift (to vertical) after the third transect. The "right" traverse is interrupted by a previous U-series sampling location (Fig. 2C). The "left" traverse runs left of the central high-porosity zone and spans the missing U-series sampling interval. To minimize the influence of high-frequency outliers, LA-ICP-MS elemental time-series were smoothed using a 13-point moving median filter followed by a 13-point moving mean filter. The 13-point filter length (37.18 μm) is less than the height of the rectangular aperture and should correspond to a very small (1–2 weeks) portion of a season assuming 1–2 mm annual growth rates. Following smoothing, replicate transect time-series were found to be nearly identical, and were accordingly averaged and concatenated to compile composite "right" and "left" traverse elemental time-series. To directly compare the high-resolution LA-ICP-MS data to the coarser stratigraphic micromill sampling, LA-ICP-MS were further binned into discrete intervals corresponding to the depths and thicknesses of micromilled samples and averaged. All further figures and discussion reference this coarser-resolution LA-ICP-MS data.

For IRMS stable isotope sampling, an inverted micromill system equipped with a 0.5 mm diameter bit was used to collect speleothem calcite in consecutive 125 μm step advances ($n = 824$). Prior to collection, the surficial 100 μm of material was removed and discarded. Individual samples, corresponding to milled volumes of $125 \times 1750 \times 1500$ μm (H × W × D), were collected by scoopula and immediately transferred to clean round-bottomed, 12 mL Labco Exetainer® vials. Micromill sampling largely followed LA-ICP-MS sampling routes in five linear collection tracks (rectangular track outlines in Fig. 2), however, minor positional variations were required to avoid irregularities and disruptions within growth laminae (e.g., small pores and microphreatic cements near larger voids). After IRMS sampling, minor differences between the LA-ICP-MS and micromilling depth scales were rectified using the 46 LDs. Where each LD crossed the LA-ICP-MS tracks, the depth was set to the depth of LD intersection with the micromill depth scale. Between LDs, depths were interpolated.

For ^{14}C analyses, a handheld drill was used to collect $2 \times 4 \times 2$ mm (H × W × D) calcite samples from the back side of the WC-3 slab (high-resolution scan of sampled slab in Electronic Annex Fig. A.1). Stratigraphic positions of ^{14}C samples were transferred to the primary sampling face

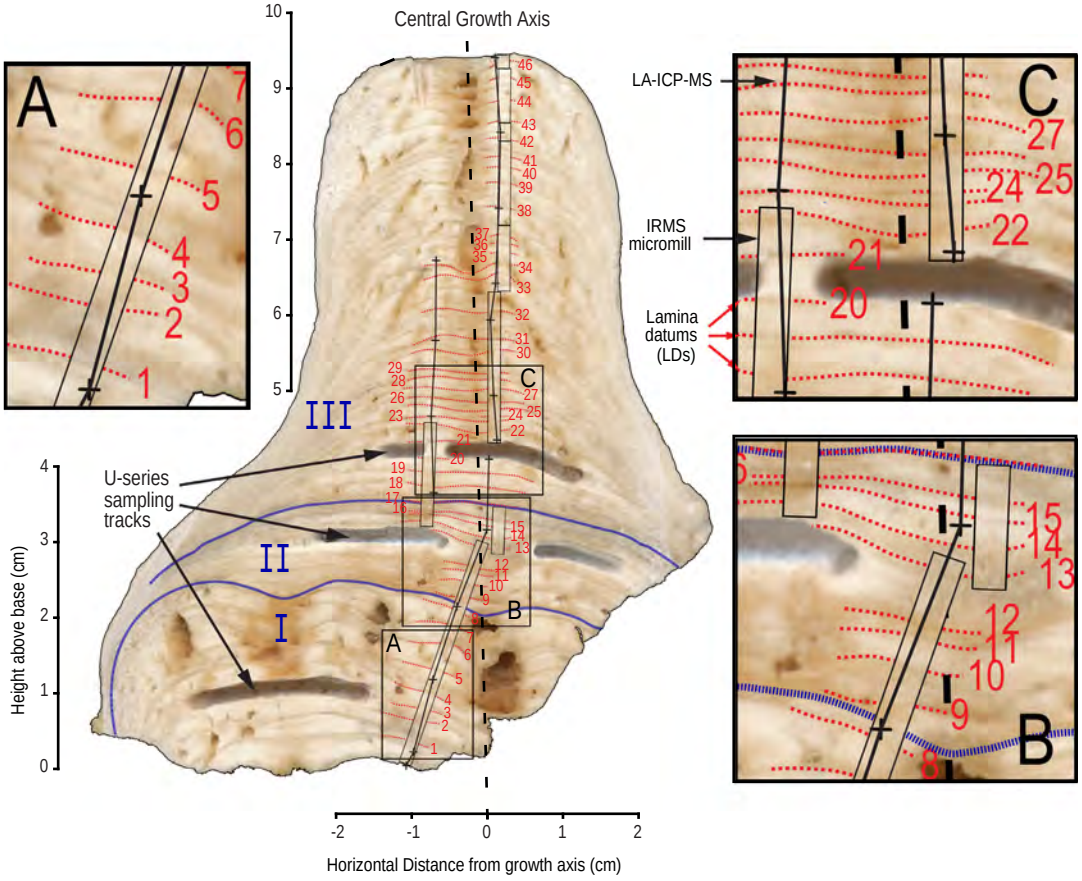

Fig. 2. High-resolution scan (2400 dpi) of a polished cross-section of stalagmite WC-3 showing: (1) persistent mm-scale laminated growth fabric about the central drip axis throughout stalagmite growth intervals (labeled I-III in blue and delineated with bold blue lines); (2) positions of LA-ICP-MS traverses (bold black lines; black crosses indicate boundaries between traverses), IRMS micromill traverses (black open rectangles), and Feng et al. (2014) U-series geochronology sampling tracks; and (3) lamina datum (LD) traces (faint red dashed lines) used to correlate LA-ICP-MS traverses with IRMS tracks. Inset views A–C are enlarged to the same scale and show detail of the sampling tracks, stalagmite lamina, and LDs. (For interpretation of the references to colour in this figure legend, the reader is referred to the web version of this article.)

for correlation with LA-ICP-MS and IRMS sampling sites, based on comparison of visually-distinctive layers between the slab faces.

3.2. Cave monitoring

Monthly cave-monitoring and sample collection procedures followed those developed for previous central Texas cave-monitoring projects (Musgrove and Banner, 2004; Banner et al., 2007; Wong et al., 2011; Cowan et al., 2013; Casteel and Banner, 2015). The monitoring in this report augments previously-reported 2009–2011 monitoring data by extending the drip water $\delta^{18}O$ data and calcite growth rate data from Feng et al. (2014) and complementing the drip water trace element data of Casteel and Banner (2015) with corresponding substrate calcite trace element measurements.

3.3. Geochemical analyses

Isotope and trace element analyses followed standard procedures (e.g., modified from McCrea (1950) and Košler (2008)). Isotope measurements were conducted by isotope-ratio mass spectrometry (IRMS) of the micromilled samples. Detailed methodology for analysis of substrate calcite trace element concentrations (solution ICP-MS), stalagmite calcite and drip water oxygen isotope composition (IRMS), stalagmite calcite radiocarbon analyses, and stalagmite trace element concentrations (LA-ICP-MS) are documented in electronic annexes. Although the IRMS method collects stable carbon isotope ratios ($\delta^{13}C$) alongside $\delta^{18}O$ values, carbon isotope values (Reported in Electronic Annex Table A5) did not exhibit regular oscillations comparable to the $\delta^{18}O$ values, so were not integrated into this study.

3.4. Construction of composite geochemical time-series

Because of the need to offset some sampling traverses/tracks laterally along the growth axis, precise comparison of IRMS and LA-ICP-MS data required a means for accurate and objective correlation between composited isotopic and elemental records. The graphical intersections of digitized lamina datum horizons (LDs) with digitized sampling

traverses/tracks (Fig. 2) provided this basis. Comparisons of $\delta^{18}O$ variations between offset IRMS tracks and positions of cross-cutting LDs were first used to compile a stratigraphic composite for IRMS data by excluding stratigraphically redundant (overlapping) data. To obtain the highest overall temporal sampling resolution, we retained the track/transect with the higher average growth rate for final compositing. A similar process was used to compile a stratigraphic composite for LA-ICP-MS data. In each case, correspondences were only confirmed after documenting comparable chemostratigraphic behavior (e.g., same number of cycles between constraining LDs; LDs cross overlapping tracks/transects at the same portion of a geochemical cycle). Final IRMS and LA-ICP-MS composite time-series are vertical base-to-top concatenations of the optimal track/transect data. The final LA-ICP-MS data composite is continuous, whereas the IRMS composite has 107 (125 μm) gaps due to insufficient sample or preparatory/analytical problems. As most gaps (104 of 107) are isolated, however, they represent a minor loss of stratigraphic information (<6–12%) relative to the typical 1–2 mm thickness of WC-3 growth layers.

3.5. Cycle-counting

From previous studies at this site, we expect to find seasonal cycles to be recorded in calcite $\delta^{18}O$, Mg, Sr, and Ba. Feng et al. (2014) found that $\delta^{18}O$ values of substrate calcite to reach local maxima during the winters, and local minima during the summers, whereas Casteel and Banner (2015) reported drip water Sr and Ba reaching local minima during the winters, and local maxima during the summers, with little variation in drip water Mg. Because only $\delta^{18}O$ values of calcite have thus far been shown at this site to respond directly and measurably to seasonal temperature changes (Feng et al., 2014), stalagmite $\delta^{18}O$ cycles in particular needed to be accurately and objectively identified and counted. We subsequently use the derived $\delta^{18}O$ cycle framework as a primary reference to compare the timing of trace element enrichment cycles.

We define cycles in the oxygen isotope record as comprising one distinct local peak ($\delta^{18}O$ maxima) and one distinct local trough ($\delta^{18}O$ minima), where each is defined by at least two IRMS measurements. This definition excludes potential single-point outliers, and establishes a minimum resolvable cycle wavelength of six IRMS measurements, or 0.75 mm. Second-order or missing peaks may be identified, as in Nagra et al. (2017), by adding optional tolerance rules to constrain the acceptable spacing and amplitude for count-worthy $\delta^{18}O$ cycles. Specifically, we considered $\delta^{18}O$ maximum-minimum pairs (prospective cycles) with amplitudes or thicknesses less than 50% of bracketing stratigraphic cycles as possible second-order cycles, and those with thicknesses greater than 200% of bracketing cycles to indicate possible missing cycles. Counting cycles with and without the tolerance rules provided a measure of $\delta^{18}O$ cycle count uncertainty.

Prospective trace element cycles may also be identified as consecutive local minima and maxima, above an amplitude threshold. However, compared to the $\delta^{18}O$ signal, trace element records exhibit signals with considerably more variation in amplitude and phasing, and have distinctly narrower enrichment peaks than depletion troughs. This relegated trace element cycle counting to a more qualitative basis based on visibly-discerned distinct local enrichment peaks; less distinct amplitude changes were also documented in order to provide a range of possible cycle-counting interpretations.

3.6. Empirical model of intra-annual calcite growth rates

The significant seasonal variability of substrate calcite growth rates at this site (Casteel and Banner, 2015) suggest that to achieve sub-annual resolution from an annual cycle-based chronology, we must account for intra-annual variations in calcite growth rate. Developing a model for intra-annual calcite growth rate variations also allows us to test the accuracy of our chronology against the instrumental record by tying individual stalagmite measurements to specific date ranges. In this model, we use monthly accumulation rates of calcite on glass substrates collected over the course of eight years (mg calcite per day; Feng et al., 2014; this study) to estimate a typical year of normalized calcite growth. Dividing each monthly substrate calcite growth rate by the total annual accumulation of substrate calcite accounts for inter-annual growth rate variations, as well as variations in accumulation that may have resulted from variation in substrate position/orientation. We model the normalized intra-annual growth rate as a continuous piecewise linear function with two subdomains per year. These subdomains have a boundary in the winter (lowest mean growth rate) and a boundary in the summer (highest mean growth rate). Normalized cumulative growth is the integral of this function: a quadratic piecewise function that is second-order continuous. Because these measurements have been normalized, the cumulative growth of calcite in one year is unity.

Each year, cumulative calcite growth begins at zero in winter at the minimum normalized growth rate and accelerates to the calculated maximum normalized growth rate in the summer, then decelerates back to the minimum normalized growth rate. Normalization allows us to consider this growth rate not just in terms of mg calcite per day on a 10×10 cm glass substrate, but also as expected linear extension rates along the growth axis of the stalagmite over the course of a year. Taking the inverse of this piecewise quadratic function, we can estimate intra-annual timing of calcite growth for a range of annual calcite growth rates in stalagmite WC-3. To apply this model to the stalagmite, we assign the maximum $\delta^{18}O$ value in each cycle as January 1, approximately the coldest expected day of the year. For the intervening samples, we scale the growth rate model to the stratigraphic thickness of the cycle and convert from stratigraphic depth to time.

4. RESULTS

4.1. Additional monitoring

Substrate calcite records of Mg, Sr, and Ba from August 2009 to September 2011 (Fig. 3) show seasonal variations characterized by summer enrichments and winter depletions. Mg concentrations in substrate calcite range from 2560–3160 ppm in the winters to 4250–5990 ppm in the summers. Sr concentrations range from 159–179 ppm in the winters to 242–336 ppm in the summers. Ba concentrations range from 44–63 ppm in the winters to 71–105 ppm in the summers. All three elemental records are highly correlated to each other ($r^2 > 0.9$), although the strongest correlation is between Sr and Ba (Mg vs. Sr, $r^2 = 0.906$; Mg vs. Ba $r^2 = 0.922$; Sr vs. Ba, $r^2 = 0.990$). Mg is the only substrate calcite trace element record to correlate with the $\delta^{18}O$ record from Feng et al. (2014; $r^2 = 0.417$, $p = 0.023$).

Additional monthly measurements of substrate calcite growth rates (Fig. 3 reinforce the seasonal trends reported in Casteel and Banner (2015), with higher summer growth rates (median 17.5 mg/day) than winter growth rates (median 9.5 mg/day). Additional measurements of drip water oxygen isotope composition (Fig. 3) continue to show a small range (−4.74 to −4.06‰ VSMOW) of variation, without regular seasonality, as first documented by Feng et al. (2014).

4.2. Macroscopic features and petrography

Macro-and microscopic characteristics of growth lamina observed in stalagmite WC-3 are shown in Figs. 2 and 4. Growth lamina are easily distinguishable in the vertical slab face as alternations between couplets of: (1) translucent, caramel-colored sparitic laminae (0.1–0.3 mm thick) and (2) thicker lighter-colored, opaque laminae (0.3–2.5 mm) (Figs. 2 and 4a). These laminae variations are respectively analogous to "dark-compact" (DC) and "white-porous" (WP) laminae commonly recognized in other fast-growing stalagmites (e.g., Genty and Quinif, 1996; Mattey et al., 2008; Boch et al., 2011), and we adopt this terminology here. Most (39 of 46) of the lamina datums used to correlate the geochemical time-series correspond to abrupt interfaces between WP and DC laminae.

Growth lamina in slab view (Fig. 2) are generally traceable across the stalagmite except in proximity to solution pores, which occur primarily along the central growth axis. These pores are often, but not always, rimmed by microphreatic (dark, translucent) calcite rinds. Lamina are thickest near the central growth axis and thin laterally away from this axis. Lamina are predominantly 1–2 mm in scale along the central growth axis, but range from sub-mm to several mm. Although distinctive in some areas of the slab face, efforts to count growth lamina throughout the vertical extent of the stalagmite were complicated by significant lateral variations in lamina thickness and consistency.

Macroscopic variations in the scale and lateral continuity of growth lamina indicate that stalagmite WC-3 developed in three phases (Intervals I-III in Fig. 2), each constructed from the two primary lamina types described above. The basal 2.2 cm (Interval I) of WC-3 consists of thick lamina couplets (3–5 mm), which are intersected by at least four mm-scale vertical pores. Laminae above and in proximity to three of these vertical pores dip inward toward each pore, suggesting these are constructional features, rather than dissolution pits. The right-most vertical pore is close to the central growth axis of the higher stalagmite, and may represent the principal enduring drip axis for WC-3. The next higher interval from 2.2 to 3.5 cm (Interval II) is characterized by lamina couplets of variable thickness (1–3 mm) that first drape across the entire growth surface without interruption by large pores. During this growth phase the stalagmite became more symmetrical and dome-shaped, although a central depression was variably expressed during this time (Fig. 2). An especially thick WP laminae in the middle of this interval, comparable to those in Interval 1, was sampled left and right of the central depression for U-series dating. At the top of Interval II, growth laminae become thinner and less distinct. The upper 6 cm of WC-3 (Interval III, 3.5–9.5 cm) contains lamina couplets 1–2 mm in thickness and is characterized by a pronounced tapering of lateral growth from a radius of about 6 cm to a radius of about 2 cm. Laminae forming near the central growth axis in the upper 4 cm of Interval III are variably separated by vertically-aligned, interconnected porosity, but otherwise can be traced laterally into flank areas.

Under microscopic inspection, porosity and fabric variations characteristic of the two types of laminae (DC and WP) have been recognized as resulting from differing degrees of lateral coalescence among smaller crystallites that form larger columnar crystals (Genty and Quinif, 1996; Boch et al., 2011). The DC and WP laminae in WC-3 are typically in optical continuity with each other (Fig. 4B and C). The thinner DC laminae are notably less-porous and may involve multiple generations of short (L generally < 100 μm; L/W ratio $< 6/1$) rhombohedral crystallites (Fig. 4D and E). Intercrystalline pores, where present, are small and spindle-shaped in cross section. More complete lateral coalescence between crystallite accretion layers approaches a palisade fabric with columnar calcite domains that are often topped by crystal terminations. WP laminae in WC-3 are characterized by an open fabric involving abundant macropores (constituting up to 50% or more by volume) between radiating-to sub-vertical elongate (L/W ratio $\gg 6/1$) columnar calcite crystals (Fig. 4D and E). Tips of elongate columnar crystals growing within some pores have regular terminations. Constituent elongate columnar calcite crystals commonly have maximum lengths spanning the entire thickness of the couplet, ranging up to at least 700 μm, and widths no greater than a few 10 s of microns, consistent with enhanced vertical growth. The orientation of macropores and elongate columnar calcite crystals principally follow the local primary growth axis of the stalagmite. Some of the thicker WP lamina contain very thin (<100 μm) horizons of compact-columnar sublaminae; some of these (7 of 46) were distinct enough laterally to serve as lamina datums.

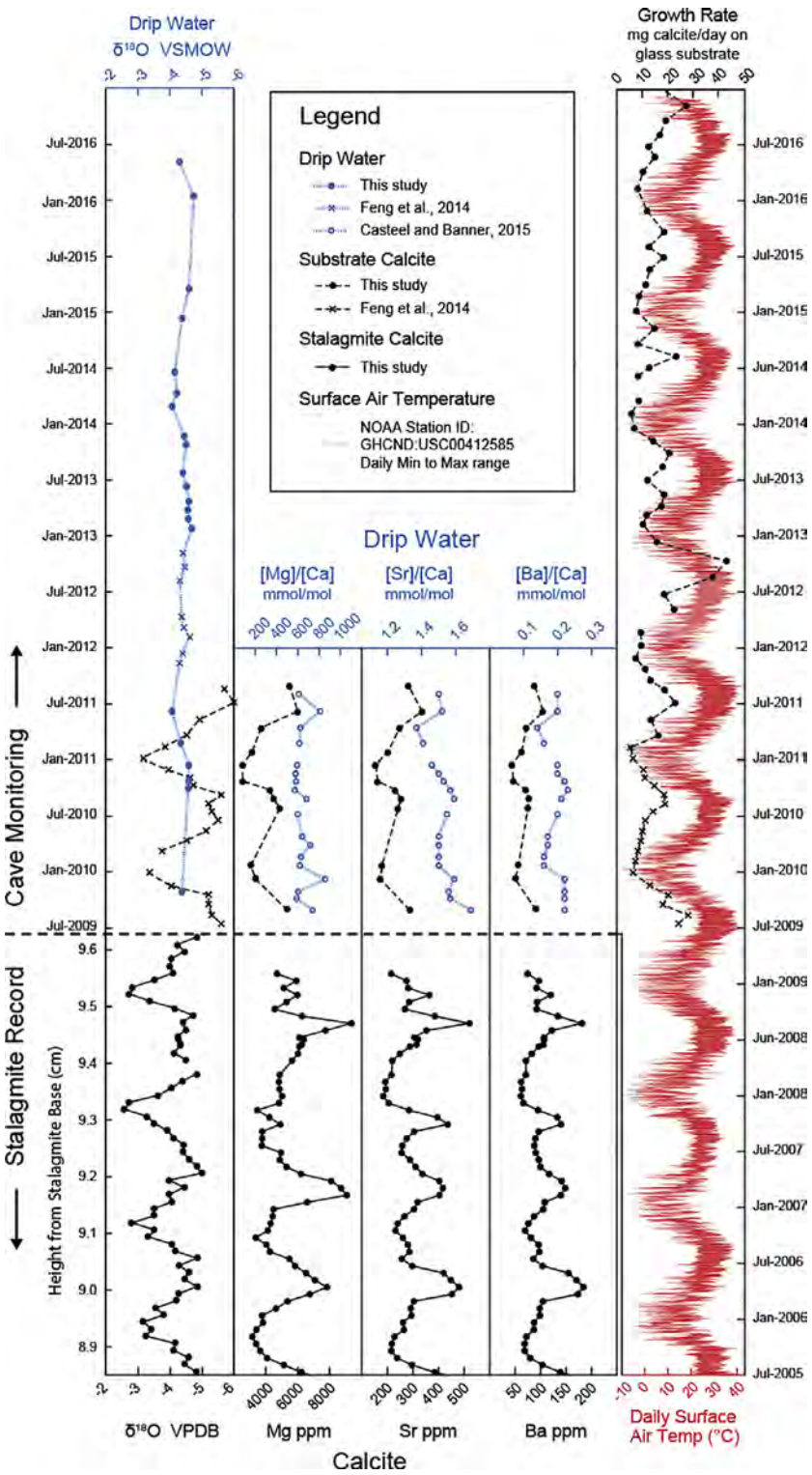

Fig. 3. Summary of preliminary cave monitoring and the top 0.8 cm of stalagmite data. Above the dashed horizontal line corresponds to the monitoring record (drip water and plate calcite), and below corresponds to the stalagmite record. The $\delta^{18}O$ axes (drip water and calcite) have been reversed to align $\delta^{18}O$ minima with trace element peaks. Variations in drip water $\delta^{18}O$ values (Feng et al., 2014 and This Study) and [Mg]/[Ca] (Casteel and Banner, 2015) are insufficient to explain variations in calcite $\delta^{18}O$ (Feng et al., 2014) or Mg compositions (This Study). Drip water [Sr]/[Ca] and [Ba]/[Ca] (Casteel and Banner, 2015) show similar seasonal variability that may explain seasonal variability observed in calcite Sr and Ba (This Study). Growth rates (Feng et al., 2014 and This Study) are average daily calcite growth on 10 cm × 10 cm sanded glass substrates. Daily surface temperature maximums and minimums (red lines) are recorded at a nearby weather station (NOAA Station ID: GHCND:USC00412585). Figure data are tabulated in the Electronic Annex, Tables A2 and A3. (For interpretation of the references to colour in this figure legend, the reader is referred to the web version of this article.)

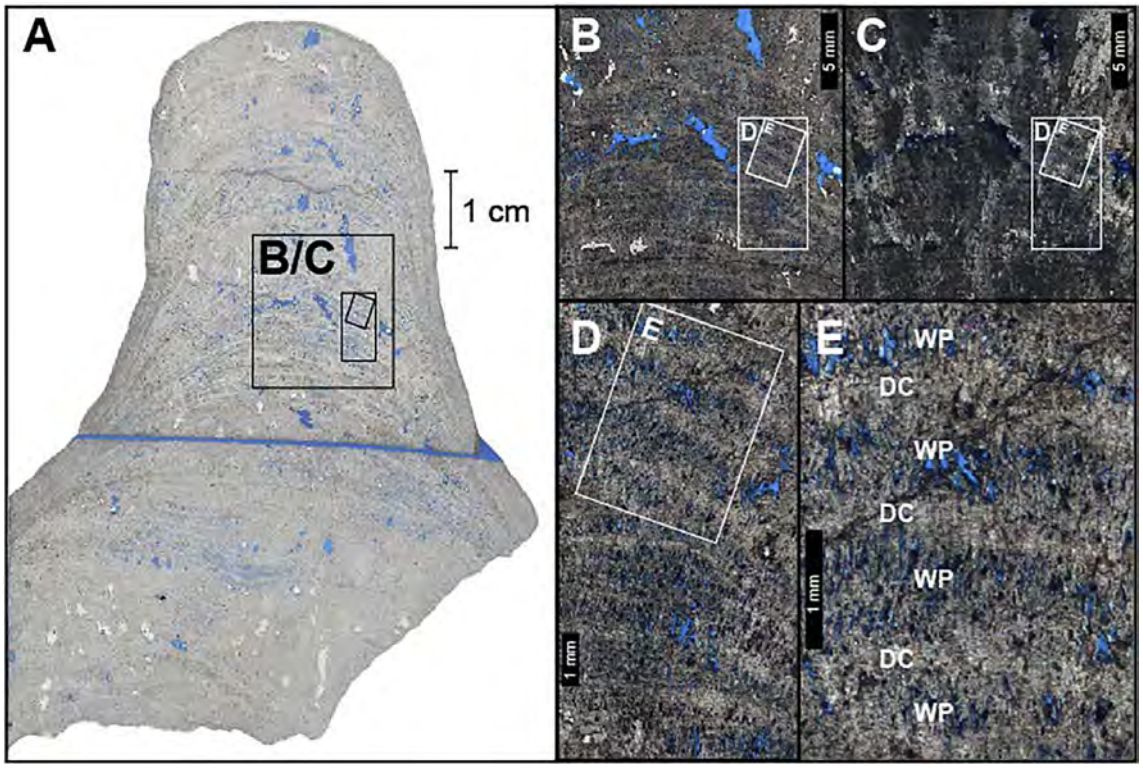

Fig. 4. Petrographic features of mm-scale calcite growth lamina in stalagmite WC-3. A. Digital scan of oversized thin sections from the slab directly opposite the primary slab (Fig. 2) sampled for $\delta^{18}O$ and trace elements. Blue epoxy shows areas of effective porosity (aside from horizontal saw cut). B/C. Corresponding plane- (B) and cross- (C) polarized light images from central medial portion of WC-3, demonstrating that lamina develop in optical continuity along the principal growth direction. D/E. Enlarged plane-polarized light views (from B) show growth lamina comprise alternating couplets of dense calcite, featuring one or more generations of compact columnar calcite (DC) with thicker and more porous calcite, featuring well-developed elongate columnar calcite (WP). Scale bars in D/E are 1 mm. The DC and WP abbreviations correspond to macroscopic characteristics previously noted for fast-growing stalagmites in slab-view (e.g., Genty and Quinif, 1996; Mattey et al., 2008; Boch et al., 2011), wherein the thinner denser couplets tend to be darker, translucent and sparitic (Dark Compact = DC) and the thicker porous couplets tend to be lighter colored (white), and opaque (White Porous = WP); cf. Fig. 2. (For interpretation of the references to colour in this figure legend, the reader is referred to the web version of this article.)

4.3. Chemostratigraphy

Stratigraphic variations among the four measured stalagmite chemical parameters ($\delta^{18}O$, Mg, Sr, Ba) are shown in Fig. 5. By treating the LDs (horizontal red lines in Fig. 5) as fixed points, the depth axis for the trace element records has been adjusted (by maximum 1 mm) to match the depth axis of the $\delta^{18}O$ record. This allows the trace element records to be directly correlated to the oxygen isotope record. All four parameters show potential cyclicity throughout the length of the stalagmite. We count 51–53 cycles in the $\delta^{18}O$ and Mg records, and 63–95 enrichment peaks in the Sr and Ba records.

4.3.1. $\delta^{18}O$ stratigraphy

Calcite $\delta^{18}O$ values range from −6.6 to −2.6‰ VPDB, with typical cycle amplitudes of 1.91 ± 0.45‰ VPDB (1σ) and stratigraphic thicknesses of 1.86 ± 0.64 mm (1σ). These findings are consistent with previously reported $\delta^{18}O$ values for the top 6.7 mm of stalagmite WC-3 (cycle amplitudes of 1.5–2.0‰ VPDB; Feng et al., 2014), but amplitudes are smaller than those observed for $\delta^{18}O$ cycles in calcite grown on artificial substrates under the same drip site over ~two years (2.3–2.9‰ VPDB; Feng et al., 2014). The long-term mean $\delta^{18}O$ value shifts stepwise along the length of the stalagmite. From 0 to 1.65 cm, the stalagmite has a mean $\delta^{18}O$ value of −4.13 ± 0.68‰ VPDB, from 1.65 to 4.15 cm a mean $\delta^{18}O$ value of −5.00 ± 0.66‰ VPDB, and from 4.15 cm to 9.5 cm a mean $\delta^{18}O$ of −4.16 ± 0.64‰ VPDB (± 1σ). Amplitudes of the cycles remain similar (1.91 ± 0.42, 1.82 ± 0.38, and 1.95 ± 0.49‰ respectively; 1σ), despite the shifts in mean $\delta^{18}O$ values. Cycle thicknesses are more variable and systematically decrease (2.31 ± 0.10, 2.15 ± 0.06, and 1.67 ± 0.05 mm, respectively; 1σ) toward the top of the stalagmite.

Throughout the stalagmite, the $\delta^{18}O$ minima in each cycle tend to be thicker (0.48 ± 0.36 mm; 1σ) than the $\delta^{18}O$ maxima (0.25 ± 0.12 mm; 1σ), with thickness of the minima or maxima defined by the $\delta^{18}O$ measurements within error of a local $\delta^{18}O$ minimum or maximum, respectively. These variations closely correspond to visible growth couplets, with $\delta^{18}O$ cycle minima associated with light-colored porous (WP) growth laminae and $\delta^{18}O$ cycle maxima associated with darker and denser (DC) laminae. Most

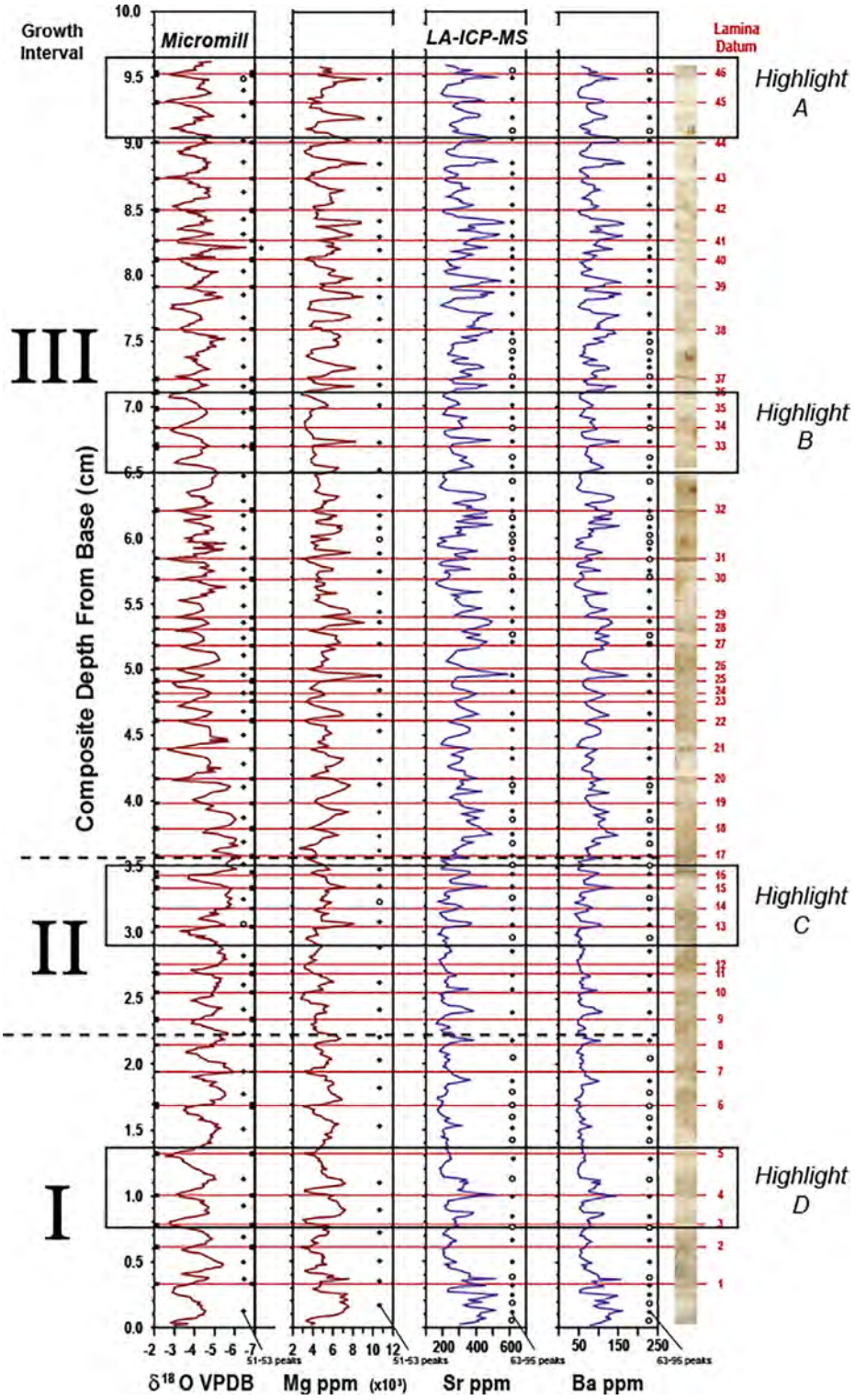
Growth Interval
Micromill
LA-ICP-MS
Lamina Datum
Highlight A
Highlight B
Highlight C
Highlight D
III
II
I
Composite Depth From Base (cm)
δ18O VPDB
Mg ppm (x10³)
Sr ppm
Ba ppm
51-53 peaks
63-95 peaks

(39 of 46) of the digitized lamina datums correspond to sharp interfaces between adjacent $\delta^{18}O$ minima and maxima.

During the counting of maxima-minima cycles in the $\delta^{18}O$ record (Section 3.5), we identified one possible missing maximum, and one potential double maximum. The possible missing maximum, from 9.38 to 9.49 cm composite depth (Fig. 5, Highlight A), has an amplitude only ~ 30% of bracketing cycles. The double maximum, from 3.01 to 3.11 cm composite depth, spans a thickness only ~30% of bracketing cycles (Fig. 5, Highlight C). We incorporate these potential ambiguities as uncertainty in the cycle-counting of the $\delta^{18}O$ chronology, where the potential missing maximum adds positive error, and the potential double maximum adds negative error resulting in a final age of 52 ± 1 cycles.

4.3.2. Trace element stratigraphies

Magnesium concentrations in stalagmite WC-3 range from 2830 to 10,900 ppm, with cycle amplitudes of several thousand ppm. Strontium concentrations range from 157 to 583 ppm, with cycle amplitudes of several hundred ppm. Barium concentrations range from 51 to 212 ppm, with individual cycle amplitudes on the order of 5–10 ppm. The trace element cycles in stalagmite WC-3 tend to manifest as enrichment peaks that are significantly thinner than the minima intervals of $\delta^{18}O$ cycles (e.g., Fig. 5, Highlight B). Some Mg enrichment peaks, however (e.g., Fig. 5, Highlight D), closely mirror the shapes and locations of $\delta^{18}O$ cycles, rather than those of Sr and Ba. Trace element enrichment peaks are somewhat suppressed during growth intervals I and II, then become more pronounced during growth interval III, with standard deviations of Mg, Sr, and Ba increasing by $19.5 \pm 3.0\%$. The mean concentrations of Sr and Ba similarly increase over this boundary, by $23.0 \pm 0.5\%$, while mean Mg concentrations remain unchanged.

Strontium and Ba enrichment-depletion patterns are particularly well correlated with each other ($r^2 = 0.972$) and less so with Mg (Sr vs. Mg, $r^2 = 0.228$; Ba vs. Mg, $r^2 = 0.253$). Although no statistically significant correlation exists between either Sr or Ba with $\delta^{18}O$ values, we find a small, but significant negative correlation between Mg and $\delta^{18}O$ values ($r^2 = 0.083$, $p \ll 0.05$). This correlation is somewhat stronger within each of the growth intervals ($r^2 = 0.14$; 0.20; 0.12, for growth intervals I, II, and III, respectively).

Overall elemental concentrations do not show any stratigraphic relationship to the shifts in mean $\delta^{18}O$ values. When cycle-counting is applied to the trace element stalagmite records, we find lower cycle counts in the Mg record (51–53 counts), and higher cycle counts in the Sr and Ba records (63–95 counts). Examples of peaks clearly visible in Sr and Ba that do not appear in the Mg record can be seen in Fig. 5, Highlights A, B, and D. Often these "extra" peaks in Sr and Ba occur at the LD intersections, though not all LD's correspond to peaks in Sr and Ba.

4.4. Radiocarbon

Stalagmite calcite ^{14}C activities ($n = 23$; Electronic Annex Table A2) begin above the threshold for initiation of atmospheric nuclear weapon testing and then increase to a peak level of 111.46% modern atmospheric ^{14}C at 4.0 cm above the base (base of interval III). Radiocarbon activities then decrease to 101.19% of modern atmospheric ^{14}C by the top of the stalagmite (collected in 2009).

5. DISCUSSION

5.1. Assessing the accuracy of $\delta^{18}O$, Mg, Sr and Ba as temperature-driven chronometers

Regular seasonal variations of substrate calcite $\delta^{18}O$ values (Feng et al., 2014), and of substrate calcite Mg, Sr, and Ba concentrations (this study), suggest each parameter as a prospective temperature-based seasonal chronometer. This monitoring, however, has occurred over a relatively limited period of time. Extending this record through the length of stalagmite WC-3 allows us to rigorously assess the reliability of each of these potential chronometers. We find enrichments in stalagmite Sr and Ba have shorter durations (are thinner) than enrichments in stalagmite Mg or $\delta^{18}O$ cycle minima, suggesting that not all four parameters are reliable annual indicators. We can, however, separate these four parameters into two groups of pairings ($\delta^{18}O$-Mg and Sr-Ba) based on the number of apparent cycles they record (52 ± 1 and 79 ± 16, respectively). Determining which, if either, of these elemental pairings is an accurate annual chronometer requires additional age constraints for the stalagmite. In order for a seasonal temperature-based chronometer to be accurate, it is furthermore crucial that the stratigraphic records considered are complete, or that any depositional hiatuses are recognized and accounted

Fig. 5. Comparison of composite $\delta^{18}O$ and LA-ICP-MS trace element records for stalagmite WC-3 growth before summer 2009 collection. The $\delta^{18}O$ axis has been reversed to align $\delta^{18}O$ minima with trace element peaks. The LA-ICP-MS depth axis has been aligned to the $\delta^{18}O$ depth axis using the LDs (horizontal red lines/numbers, refer to Fig. 2 and text; small black boxes on $\delta^{18}O$ vertical axes show maximum stratigraphic range of lamina datums intersected during micromill sampling). To the right of the geochemical data is 2400 dpi imagery of the micromill track before sampling (composite). Roman numerals and horizontal dashed lines show principal growth intervals (cf. Fig. 2). Closed circles records show countable trace element peaks and $\delta^{18}O$ cycles, whereas open circles show peaks that may or may not be countable. Highlight A shows an example of a peak appearing in the Sr and Ba records that does not appear in the $\delta^{18}O$ and Mg records (coincident with LD 45), as well as a possible double minima in the $\delta^{18}O$ record (below LD 46). Highlight B shows another example of an extra Sr-Ba peak (LD 34), along with the sharper peaks often found in the trace element record (below LD 33). Highlight C shows multiple peaks in the trace element record during a single $\delta^{18}O$ cycle (LDs 14–16), along with a possible extra $\delta^{18}O$ cycle minimum (LD 13). Highlight D shows $\delta^{18}O$ cycle minimum and Mg peak shapes differing from peak shapes in the Sr and Ba records. (For interpretation of the references to colour in this figure legend, the reader is referred to the web version of this article.)

for. Here, we discuss how these factors bear on the construction and fidelity of a seasonally-resolved age model for stalagmite WC-3.

5.1.1. Implications of substrate calcite growth rates and trace element composition

Extended monthly measurements of substrate calcite accumulation (2012–2017) at site WC-3 confirm the findings of Casteel and Banner (2015) that calcite growth rates are highest in the summer and lowest in the winter. In the stalagmite, thicker WP laminae should accordingly correspond to summer growth (high growth rate), whereas thinner DC laminae should correspond to winter growth (low growth rate). Our new trace element analyses of the same substrate calcite monitoring samples previously measured for $\delta^{18}O$ by Feng et al. (2014) reveal that Mg, Sr, and Ba enrichments tend to occur during the warm months (Fig. 3). These updated monitoring-based findings predict that chemostratigraphic variations in the stalagmite should follow the development of growth couplets, with enrichments in Mg, Sr, and Ba concentrations and minima in $\delta^{18}O$ values coinciding with thicker WP laminae, and the inverse coinciding with thinner DC laminae. We find that this prediction is validated, but exceptions do exist, with some peaks in Sr and Ba occurring in DC laminae, and some DC sub-laminae occurring during $\delta^{18}O$ minima.

5.1.2. Numeric age constraints

Three U-series ages of 70 ± 13, 160 ± 20, and 50 ± 13 years before measurement were determined by Feng et al. (2014) in the lower half of stalagmite WC-3 (10 mm, 30 mm, 45 mm from the bottom, respectively). These ages correspond to dates of 1940, 1850, and 1960 CE, respectively, using the bulk earth $^{230}Th/^{232}Th$ composition of 4.4 ppm and an uncertainty of 100% for the initial Th correction (e.g., Dorale et al., 2004). Feng et al. (2014) interpreted the resulting age reversal to variations in detrital Th compositions through time. Initial $^{230}Th/^{232}Th$ ratios of 6.0, 10.8, and 9.0 ppm are required to provide U-series ages consistent with the $\delta^{18}O$- and Mg-derived chronologies. Aberrant U-series ages could potentially result from U loss associated with the porous nature of stalagmite WC-3, particularly the thicker WP laminae sampled for dating, even if seasonal signals in $\delta^{18}O$ values and trace element concentrations were retained (Bajo et al., 2016). Because of these high uncertainties, the only reasonable interpretation of the U-series ages is that they are consistent with the lower portion of stalagmite WC-3 growing during the 20th century.

Improved age constraints are provided by carbon-14 activity measurements of stalagmite WC-3, which resolve the atmospheric ^{14}C peak (i.e., bomb pulse) recorded in the stalagmite, and demonstrate that growth began after the onset of 20th century nuclear weapons testing (i.e., Genty et al., 1998, 1999, 2001a,b). In the atmosphere, this pulse of $^{14}CO_2$ was first clearly observable in 1955 (Fig. 6), and peaked in 1963 at about 200% modern atmospheric ^{14}C (Hua et al., 2012, 2013). The ^{14}C activity measured at the base of the stalagmite thus indicates that initial growth began no earlier than 1955. Highest ^{14}C activity levels occur at 4.0 cm above the base of the stalagmite, with

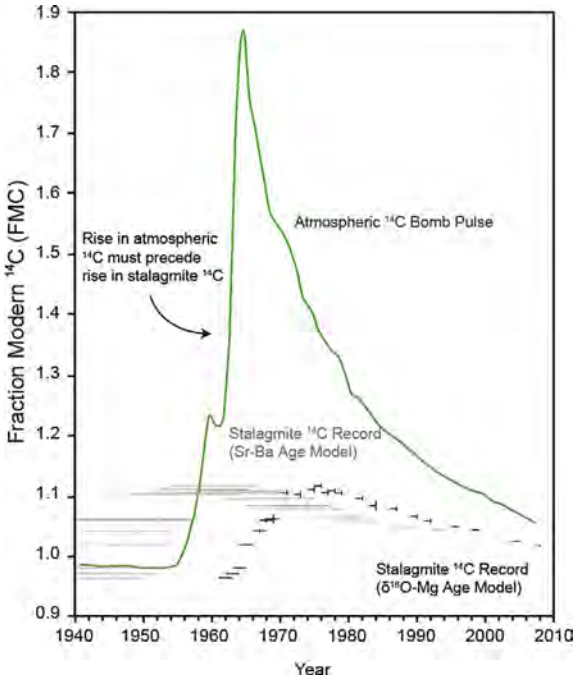

Fig. 6. WC-3 ^{14}C measurements, in fraction modern carbon (FMC), plotted against stalagmite growth year, as determined by $\delta^{18}O$ and Mg age model (black crosses) and the Sr and Ba age model (gray crosses). Radiocarbon measurement error is shown as the height of each cross, whereas age model error is shown as the width of each cross. Also plotted is the Northern-Hemisphere atmospheric ^{14}C bomb peak, in FMC (green line; Levin et al., 1994). The sharp rise in atmospheric ^{14}C provides a lower bound for stalagmite growth: the rise in ^{14}C observed in the base of stalagmite WC-3 cannot precede the rise of atmospheric ^{14}C that began in 1955. Because all interpretations of the Sr and Ba age model show a rise in stalagmite ^{14}C preceding the atmospheric rise in ^{14}C, the Sr and Ba age model cannot be correct. (For interpretation of the references to colour in this figure legend, the reader is referred to the web version of this article.)

an inflection toward slower rates of increase at 3.1 cm. Variable residence times and mixing of carbon in the epikarst will lead to a lag, attenuation, and spreading of the atmospheric bomb pulse in stalagmite records (i.e., Genty et al., 1998, 1999; 2001a,b; Hodge et al., 2011; Noronha et al., 2015). The $\delta^{18}O$-Mg age model indicates a basal age of 1956–58 (winter), 1–3 years after initiation of atmospheric nuclear weapons testing, whereas the prospective Sr-Ba age model indicates a basal age of 1914–1946, 9–41 years before initiation of testing. Fig. 6 compares the timing of radiocarbon activities to the proposed $\delta^{18}O$- and Mg-derived age model. Only the $\delta^{18}O$-Mg age model is compatible with the radiocarbon age constraints, and thus it is most likely to proxy temperature seasonality. The higher numbers of enrichment peaks for Sr-Ba are thus likely driven by factors in addition to seasonal temperature variations.

5.1.3. Continuity of the geochemical time-series

A cycle-based geochemical chronometer is only accurate insofar as the record is continuous and uninterrupted. We

identify three primary mechanisms that could lead to unrecorded seasonal cyclicity in the stalagmite: (1) gaps from unsuccessful IRMS analyses, (2) growth hiatuses, and (3) stratigraphic aliasing during sampling.

The 107 gaps in the IRMS data due to failed analyses are thin (<6–12%) compared to thicknesses of typical growth lamina (1–2 mm) and are therefore unlikely to lead to miscounting of annual peaks.

In general, long-term hiatuses in stalagmite growth can be identified by petrographic analysis as micritic layers, detrital-rich layers, or dissolution surfaces (Tan et al., 2006). No evidence for hiatuses were identified by petrographic inspection. As the site continued dripping and precipitating calcite through the most severe drought in Texas recorded history (2011; Nielsen-Gammon, 2012), it is unlikely that less-severe earlier droughts would have stopped stalagmite growth.

The greater sampling footprint of the micromill compared to the laser means the IRMS $\delta^{18}O$ data were most prone to aliasing. Some degree of aliasing will unavoidably occur wherever growth layers are non-orthogonal to the axis of the sampling track, either laterally or with depth. This will have the effect of attenuating or widening maxima and minima in the $\delta^{18}O$ data. If multiple annual lamina are intersected during collection of a single micromill sample, $\delta^{18}O$ cycles will be masked by averaging. This would appear as multiple adjacent IRMS samples recording $\delta^{18}O$ measurements near the mean annual $\delta^{18}O$ value, and is not observed in our data. Because the wider IRMS drilling track was not precisely centered on the LA-ICP-MS laser traverse, it is more likely that local variations in the dip of growth lamina results in trace element features that are slightly offset from equivalent correlation points in the oxygen isotope data. The number of times each LD was intersected by discrete micromill samples is a gauge of this aliasing potential. This number ranges between 1 and 5 (0.125–0.625 mm), with a median of 2 (0.25 mm), among the 46 digitized LDs, indicating that micromill stratigraphic aliasing was mainly on the order of 13–25% of typical WC-3 growth lamina thicknesses of 1–2 mm, and therefore unlikely to cause undercounting of annual cycles.

5.2. Controls on oxygen-isotope cycles

The wide range of seasonal temperature variations in temperate latitude settings could serve as a consistent annual chronometer, if faithfully recorded by environmental proxies. At Westcave, Feng et al. (2014) found that seasonally varying surface temperatures were the primary control on substrate calcite $\delta^{18}O$ variations over the monitoring period, and on four $\delta^{18}O$ cycles identified in the top 6.7 mm of stalagmite WC-3. To further test their conclusion, we compare the 52 ± 1 $\delta^{18}O$ cycles resolved in the full length of stalagmite WC-3 and assign them as years before 2009. We then compare $\delta^{18}O$ values to daily instrumental weather records from 1957–2009 in Austin, TX, the most comprehensive local weather records available for this time period (NOAA station ID: GHCND:USW00013958). We apply the empirical calcite growth model to the stalagmite $\delta^{18}O$ cycle stratigraphy in order to convert stratigraphic depth to estimated dates of calcite growth for every micromill sample. Annual least-squares regressions of sample $\delta^{18}O$ values versus mean Austin temperature over the inferred sampling periods allow us to test the robustness of the relationship between temperature and stalagmite $\delta^{18}O$ values (Fig. 7). Using the fifty full-year records, we find that regression line slopes vary over a small range from −0.12 to −0.05‰/°C, and can be approximated by a normal distribution with a mean of −0.08‰/°C and a standard deviation of 0.03‰/°C (Kolmogorov-Smirnov test, $\alpha = 0.05$). When we compare the Feng et al. substrate calcite $\delta^{18}O$ values to average Austin temperatures over their respective periods of calcite growth, we find a similar slope of −0.09‰/°C, suggesting similar temperature controls on both systems. These slopes are related to, but shallower than, the slopes reported for various equilibrium or near-equilibrium calcite-water fractionation experiments (e.g., −0.21‰/°C, Kim and O'Neil, 1997; −0.177‰/°C, Tremaine et al., 2011). This discrepancy is at least partially explained by the greater temperature extremes recorded at the surface (7–32 °C, 30-day means, 2009–2017) than in cave drip water (8–26 °C, monthly spot measurements, 2009–2017). Other factors are likely less significant. These could include the effects of seasonally-biased calcite growth rate effects on $\delta^{18}O$ fractionation, seasonally-enhanced evaporative effects on the $\delta^{18}O$ values of drip water, seasonally-enhanced biotic calcite precipitation, or diagenesis. The regular nature of the $\delta^{18}O$ cycles and the relative invariance of drip water $\delta^{18}O$ rule out a diagenetic control on $\delta^{18}O$ cycles (e.g., Demény et al., 2016). This near-entrance environment is likely microbially active, which would likely lead to enhanced calcite precipitation (Banks et al., 2010), but seasonal changes in biotic effects may enhance seasonality in $\delta^{18}O$ values. The stalagmite shows no coralloid morphology, so evaporation did not likely play a significant role in speleothem growth (Caddeo et al., 2015). If evaporation affects stalagmite $\delta^{18}O$ values, it would likely lead to higher $\delta^{18}O$ values in summers than in winters, which is opposite from the observed trend. While growth-rate effects on calcite $\delta^{18}O$ fractionation may be a factor, the growth rate itself depends strongly on cave temperature. Despite these potential confounding effects, a significant correlation to seasonal temperature remains for every annual regression line ($r^2 = 0.46$–0.96 for the 50 annual regression lines), and this aggregate relationship closely mirrors that observed in the substrate calcite. Altogether, this suggests that seasonal temperature variations are the primary control on stalagmite $\delta^{18}O$ variations, thus supporting the interpretation of $\delta^{18}O$ cycles as annual and supporting their use as a chronometer (Fig. 8).

5.3. Controls on magnesium cycles

We compare monthly measurements of drip water [Mg]/[Ca] to coeval monthly measurements of substrate calcite Mg (Casteel and Banner, 2015). We find that published Mg partition coefficients ($D_{Mg} = (Mg/Ca)_{calcite}/(Mg/Ca)_{solution}$; Huang et al., 2001; Huang and Fairchild, 2001) significantly over-estimate the Mg composition expected for the stalagmite. Apparent D_{Mg} values for

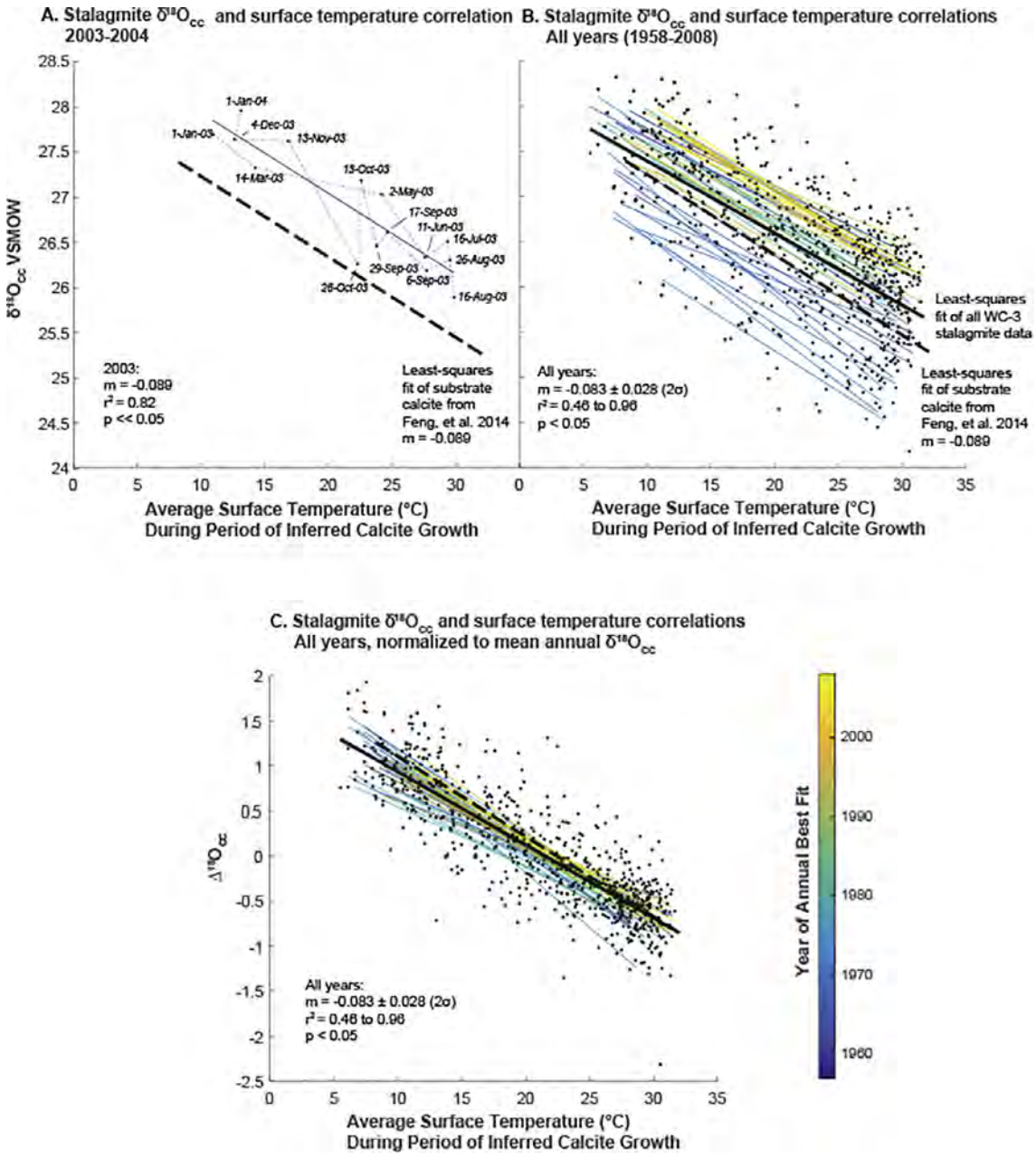

Fig. 7. A. Oxygen isotope composition versus average surface temperature for inferred stalagmite growth in 2003. Points are individual measurements, labelled with their inferred average growth date. Maximum $\delta^{18}O$ values in a cycle are assigned 1-Jan, and minimum $\delta^{18}O$ values are assigned 16-Aug. Samples between these two dates are interpolated using an empirical non-linear growth rate model. The labeled date is the average date for the interpreted period of calcite growth for each sample. A least-squares fit line (blue) for 2003 is plotted, as well as a least-squares fit for all substrate calcite (black, dashed). B. All stalagmite $\delta^{18}O$ values. Annual best fit lines are color-coded by year. Also plotted: least-squares fit for all substrate calcite data (black, dashed) and least-squares fit for all stalagmite data (black, solid). C. All stalagmite data, normalized to each year's median $\delta^{18}O$ values, plotted as $\Delta^{18}O$. This shows the sensitivity of stalagmite and substrate calcite $\delta^{18}O$ values to surface temperature. Also plotted: least-squares fit for all substrate calcite data (black, dashed), and least-squares fit for all stalagmite data, (black, solid). (For interpretation of the references to colour in this figure legend, the reader is referred to the web version of this article.)

substrate calcite at this site (0.007–0.015) show lower temperature sensitivity (0.00025/°C, $r^2 = 0.65$, $p \ll 0.05$) than previously published D_{Mg} values (~0.0008/°C; Huang et al., 2001; Huang and Fairchild, 2001). When the range of stalagmite Mg values is compared to the median drip water [Mg]/[Ca] over the monitoring period, the apparent D_{Mg} values range from 0.009 to 0.024. This is still lower than published D_{Mg} values, but assuming the high Mg

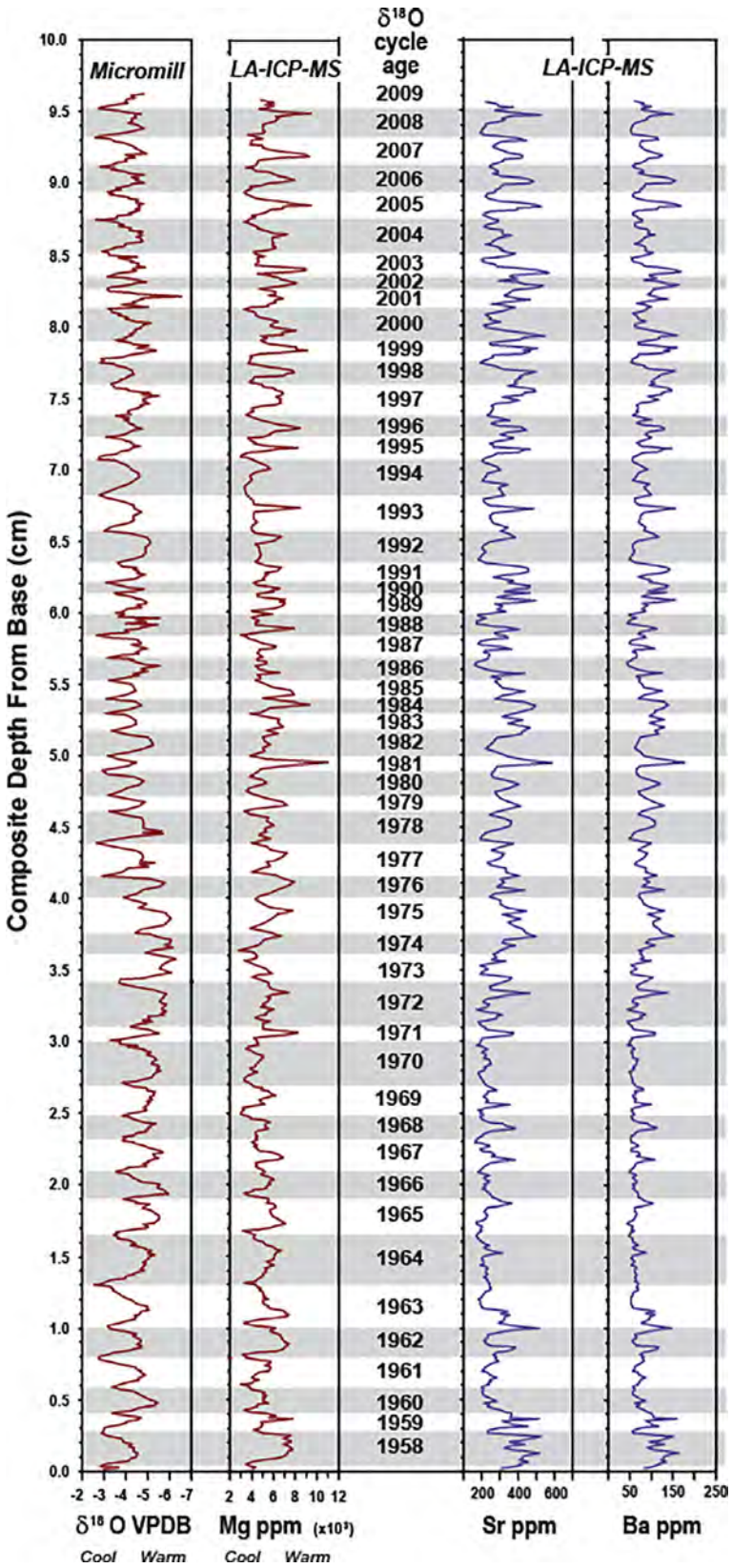

Fig. 8. Comparison of composite $\delta^{18}O$ and LA-ICP-MS time-series for stalagmite WC-3 growth before summer 2009 collection. Alternating grey and white bands show interpreted $\delta^{18}O$ cycle years. The $\delta^{18}O$ axis has been reversed to align $\delta^{18}O$ minima with trace element peaks.

concentrations in the stalagmite correspond to high temperatures in the cave, as they do in the substrate calcite, the temperature sensitivity of D_{Mg} would be 0.00074/°C, similar to previously published D_{Mg} values (~0.0008/°C; Huang et al., 2001; Huang and Fairchild, 2001).

Due to the proximity of this stalagmite to cave entrances, and the well-ventilated nature of the cave, we must consider the possibility that aeolian particulates might contribute Mg to the surface of the growing stalagmite (e.g., Belli et al., 2017). We find this to be an unlikely explanation in this setting, as calcite Mg concentrations are lower than predicted by drip water [Mg]/[Ca], and aeolian deposition of high-Mg particulates would increase stalagmite Mg concentrations. Likewise, variable drip water [Mg]/[Ca], due to prior calcite precipitation (PCP; e.g., Fairchild et al., 2000; Treble et al., 2003; Cruz et al., 2007; Sinclair et al., 2012), incongruent calcite dissolution (ICD; e.g., Sinclair et al., 2012; Belli et al., 2017), or water-rock residence time in the epikarst (Treble et al., 2003) could account for variations in stalagmite Mg concentrations, but variations in drip [Mg]/[Ca] over the monitoring period do not correlate with variations in substrate calcite Mg concentrations (Casteel and Banner, 2015). Although we cannot rule out water-rock interactions as the primary control for the unmonitored period of stalagmite growth, the strong correspondence between $\delta^{18}O$ cycle minima and Mg peaks (Fig. 8) suggests that temperature is the primary control on calcite Mg variability.

5.4. Controls on strontium and barium cycles

The consistently strong correlation between stalagmite Sr and Ba concentrations (Fig. 8) suggests that the same processes control both trace element records. Comparing substrate Sr variations to drip water [Sr]/[Ca] variations, we calculate partition coefficients of 0.05–0.10, similar to previously published D_{Sr} values (e.g., Lorens, 1981; Banner, 1995; Tesoriero and Pankow, 1996). Unlike D_{Mg} coefficients, D_{Sr} and D_{Ba} coefficients are not expected to vary with temperature. Previous studies have found D_{Sr} to vary with calcite growth rate, increasing by 0.05–0.1 with a ten-fold increase in growth rates (Lorens, 1981; Tesoriero and Pankow, 1996; Huang and Fairchild, 2001; Belli et al., 2017). The growth rates of stalagmite WC-3, as estimated from calcite growth on glass substrates or as linear extension rates of the stalagmite itself, are far faster than the calcite growth rates used in the aforementioned studies, thereby limiting the utility of direct comparisons of D_{Sr} coefficients between this and previous studies. We do find that while our calculated D_{Sr} coefficients are far lower than would be expected from extrapolation of previous studies to our higher growth rates, the sensitivity of our calculated glass substrate D_{Sr} coefficients to growth rate (0.050 per ten-fold increase in growth rate, $r^2 = 0.48$, $p \ll 0.05$) is similar to previously-published D_{Sr}-growth rate relationships. Mucci and Morse (1983) found a strong dependence of D_{Sr} on Mg/Ca in the solution, but this is unlikely to be a primary control on WC-3 stalagmite Sr concentrations, given the lack of correlation between drip water [Mg]/[Ca] and substrate calcite D_{Sr} during the monitoring period ($r^2 = 0.15$, $p > 0.05$). Sr and Ba concentrations in the substrate calcite do correlate weakly to calcite growth rate on the glass substrate ($r^2 = 0.30$, $p = 0.064$; $r^2 = 0.28$, $p = 0.074$), suggesting that growth rate is a primary control on calcite Sr and Ba concentrations at this site.

Drip water [Sr]/[Ca] and [Ba]/[Ca] have stronger correlations to calcite growth rate ($r^2 = 0.35$, $p = 0.0092$; $r^2 = 0.38$, $p = 0.0062$). The possible controls on variations in drip water [Sr]/[Ca] and [Ba]/[Ca] are similar to that of drip water [Mg]/[Ca]: PCP (Treble et al., 2003; Sinclair et al., 2012), incongruent calcite dissolution (ICD; Sinclair et al., 2012; Belli et al., 2017), or water residence time (Treble et al., 2003; Fairchild and Treble, 2009; Wong et al., 2011). These, however, are all expected to have a similar effect on the relative concentrations of Mg, Ba, and Sr to Ca (Sinclair et al., 2012), and while [Sr]/[Ca] and [Ba]/[Ca] in the drip waters were found to co-vary, [Mg]/[Ca] did not follow the same seasonal trends. Casteel and Banner (2015) found that a combination of PCP, ICD, and water-rock interactions (WRI; a broad term for recrystallization and dissolution processes that excludes pure PCP and ICD) can explain the covariance of [Ba]/[Ca] and [Sr]/[Ca] at WC-3. They further suggested that PCP dominated in the summer, and ICD/WRI dominated in the winter, but did not explain the relative lack of seasonality in drip water [Mg]/[Ca] using the same models.

A study of an annually-laminated speleothem by Roberts et al. (1998) provides a possible mechanism to explain the decoupling of drip water [Mg]/[Ca] from [Sr]/[Ca] and [Ba]/[Ca]. They found that if the epikarst host rock contains calcite and dolomite, that incongruent dolomite dissolution, could account for antiphase behavior of Mg and Sr. In such systems, high-Sr calcite will dissolve first, driving up [Sr]/[Ca]. As the water approaches calcite saturation, the dissolution of low-Sr, low-Ba dolomite will drive the simultaneous precipitation of calcite, thereby lowering Sr and Ba concentrations increasing Mg concentrations in the stalagmite. If the winter-time ICD/WRI at Westcave found by Casteel and Banner (2015) includes incongruous dolomite dissolution, this could drive drip-water Mg concentrations up and Sr and Ba concentrations down in the winter or spring, while PCP drives all three trace elements to high concentrations in the summer.

This variation in drip water [Sr]/[Ca] and drip water [Ba]/[Ca], combined with variable calcite growth rates controlling D_{Sr} and D_{Ba}, may explain the cyclical Sr and Ba concentrations observed in stalagmite WC-3. While Casteel and Banner (2015) found that calcite growth rates at this site are driven by changes in temperature, it is also possible that in some years, changes in epikarst pCO_2 or drip water [Ca] could alter calcite growth rates, causing enrichments or depletions in calcite Sr and Ba concentrations that are decoupled from temperature.

5.5. Implications for paleoclimate reconstruction

The distinct temperature seasonality recorded by $\delta^{18}O$ values, Mg concentrations, and growth rates for substrate calcite grown at site WC-3 highlight the importance of modern cave monitoring studies for interpreting

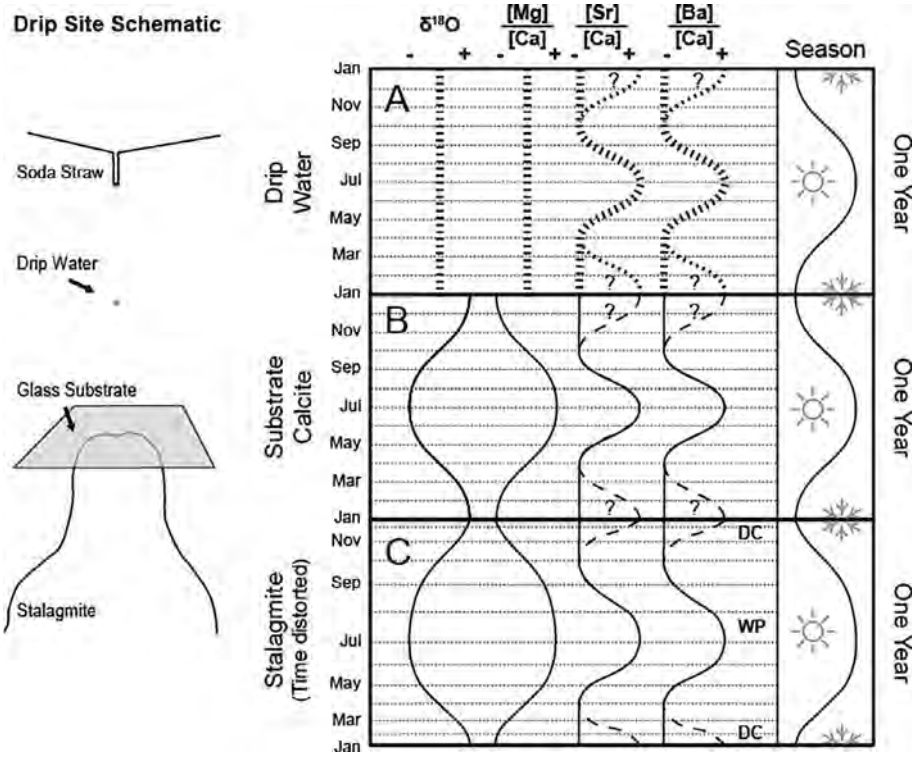

Fig. 9. Summary of annual geochemical variations in drip water, substrate calcite deposition, and stalagmite growth for the WC-3 near-entrance cave environment, as realized from integrated monitoring and stalagmite chemostratigraphic analysis. Perspectives from a two-year monitoring interval (2009–2011) indicate: A. *Drip-water* $\delta^{18}O$ values (Feng et al., 2014) and [Mg]/[Ca] (Casteel and Banner, 2015) are relatively invariant with no obvious seasonal expression, whereas [Sr]/[Ca] and [Ba]/[Ca] vary seasonally (Casteel and Banner, 2015). B. *Substrate calcite* records seasonal variations in $\delta^{18}O$ values (with summer minima; Feng et al., 2014) and [Mg]/[Ca], [Sr]/[Ca] and [Ba]/[Ca] (with summer maxima). Substrate calcite growth rates (not shown) are highest during summers and lowest during winters. Continued monitoring (2012–2017; This study) of drip water $\delta^{18}O$ values and plate calcite growth supports the former observations. C. *Stalagmite calcite* exhibits regular stratigraphic fluctuations in $\delta^{18}O$ values and [Mg]/[Ca], with amplitudes comparable to the seasonal $\delta^{18}O$ and [Mg]/[Ca] variations documented for substrate calcite (2009–2011). This consistency supports that stalagmite $\delta^{18}O$ and [Mg]/[Ca] effectively log seasonal temperature variations in this setting, due to the temperature-sensitivity of oxygen-isotope fractionation and Mg partitioning between water and calcite. Although stalagmite [Sr]/[Ca] and [Ba]/[Ca] variations also mimic those recorded in substrate calcite (2009–2011), the longer stalagmite record demonstrates that the timing of [Sr]/[Ca] and [Ba]/[Ca] peaks does not necessarily correspond with maximum summer air temperature ($\delta^{18}O$ minima, [Mg]/[Ca] maxima) and that sub-seasonal [Sr]/[Ca] and [Ba]/[Ca] peaks occur in certain years. Analyses of substrate calcite and drip water over a longer monitoring interval are predicted to reveal sub-seasonal Sr and Ba enrichments (labelled with question marks). The timing of distinct growth lamina development in stalagmite WC-3 are interpreted from plate calcite growth rate monitoring (2009–2017), with DC couplets corresponding to decreased winter calcite growth and WP couplets related to increased summer calcite growth (see Fig. 2, Fig. 4). The variable growth rates for seasonal couplets result in condensed winters and expanded summers within the stalagmite chemostratigraphy. Because the drip water and substrate calcite records are collected at regular time intervals, they do not experience the same time distortion.

speleothem geochemical records. Although previous studies have used radiometric age constraints (e.g., ^{14}C, U-series, or ^{210}Pb dating) to verify seasonal geochemical cycles in stalagmites (e.g., Baskaran and Iliffe, 1993; Mattey et al., 2008; Nagra et al., 2017), only studies that include cave monitoring (e.g., Frisia et al., 2000) or cave proxy system modelling (e.g., Genty et al., 2001a,b) can establish how cycle components (maxima and minima) specifically relate to winters and summers, and how calcite growth fabrics vary seasonally.

In the case of stalagmite WC-3, cave monitoring demonstrates that calcite growth in this near-entrance setting is fundamentally different from stalagmites forming in deeper caves in the region. The set of conditions in Westcave that also characterize the near-entrance environments of temperate caves (i.e., low cave air P_{CO2} and seasonally-variable temperatures), combined with low variability in drip water $\delta^{18}O$ and Mg values provide two complementary temperature-linked seasonal chronometers. While this study focused on an actively growing stalagmite with a known collection age, integration of geochemical cycle-counting with traditional U-series dating could potentially allow for records of temperature or precipitation seasonality to be derived from near-entrance stalagmites that are not actively growing or that encompass time intervals of particular paleoclimate interest.

Near-entrance environments are more vulnerable to weathering, biological interference, and diagenetic alteration, however, and therefore are likely to provide shorter records than deep-cave environments. The niche

for near-entrance speleothem proxy records (e.g., stable isotope, trace elements, or wind-deposited records) is most likely for decadal- to centennial-scale paleoclimate applications, complementing instrumental records and other high-resolution terrestrial proxies (e.g., dendroclimatological records, lake varves, and ice core records). If a precise temperature proxy is to be developed from speleothems, then near-entrance and other well-ventilated cave sites are those most likely to record accurate seasonal temperatures. Developing precise and accurate sub-annual chronologies of stalagmites in such sites is a crucial first step towards more paleoclimatic goals.

6. CONCLUSIONS

High-spatial-resolution $\delta^{18}O$ and trace element analysis of a near-entrance stalagmite, combined with modern monitoring of substrate calcite growth and drip-water geochemical composition, provide independent, temperature-based seasonal chronometers that enable a 52 ± 1 year-long age model with sub-annual resolution to be constructed. We find two pairs of isotope/chemical composition records in this near-entrance stalagmite system: $\delta^{18}O$-Mg and Ba-Sr (Fig. 9). We find the $\delta^{18}O$ and Mg calcite records to be robust chronometers of temperature seasonality in this setting, likely due to the proximity to surface air temperatures coupled with small temporal variations in drip-water $\delta^{18}O$ values and Mg concentrations. We observe and confirm this seasonality in substrate calcite records, and find pronounced, continuous seasonal $\delta^{18}O$ and Mg cycles with corresponding pseudo-seasonal enrichments in Ba and Sr concentrations in stalagmite WC-3. By comparison with the substrate calcite records, we establish that the $\delta^{18}O$ and Mg cycles in the stalagmite are annual, and correspond to seasonal variations in surface air temperature. The discrepancy in the number of cycles between the $\delta^{18}O$-Mg records and the Ba-Sr records may be explained by the primary sensitivity of the $\delta^{18}O$ and Mg records to in-cave temperature, in contrast to the primary sensitivity of the Ba and Sr records to growth rates of the stalagmite itself. Potential discrepancies between the $\delta^{18}O$ and Mg cycles could be explained by secondary sensitivity of [Mg] to P_{CO2}-driven, rather than temperature-driven prior calcite precipitation events.

Although a two-year cave monitoring interval suggested seasonal variation of calcite $\delta^{18}O$ values and Mg, Sr, and Ba concentrations, the differing numbers of enrichment-depletion cycles documented in the longer stalagmite record are inconsistent with both element pairings being accurate annual chronometers (Fig. 9). A chronology derived from the 51–53 $\delta^{18}O$ and [Mg] enrichment-depletion would be compatible with deposition between 1957 ± 1 and 2009, whereas a chronology derived from the 63–95 [Sr] and [Ba] enrichment-depletion cycles would be compatible with deposition between 1930 ± 16 and 2009. Radiocarbon measurements rule out the older basal age of 1930 ± 16, as ^{14}C levels near the base of stalagmite WC-3 show a rise of ^{14}C consistent with post-1955 atmospheric testing of nuclear weapons. For this reason, in addition to the well-documented temperature effect on $\delta^{18}O$ and [Mg] in calcite, we conclude that $\delta^{18}O$ and [Mg] are the most reliable annual chronometers in this near-entrance speleothem locality, and that [Sr] and [Ba] likely record additional climatological or hydrological variables. Near-entrance stalagmites are capable of reflecting sub-seasonal temperature variations, and thus could provide high-resolution age models over decadal to centennial scales for targeted paleoclimate studies

ACKNOWLEDGEMENTS

This research was supported by NSF REU grant EAR-1157031, NSF Geobiology and Low Temperature Geochemistry grant EAR-1124514 and by the Jackson School of Geosciences and Environmental Science Institute of the University of Texas. We wish to thank the management and staff at Westcave Preserve and many others over the past decade for assistance in the field.

APPENDIX A. SUPPLEMENTARY MATERIAL

Supplementary data associated with this article can be found, in the online version, at https://doi.org/10.1016/j.gca.2018.04.036.

REFERENCES

Allison V. C. (1926) The antiquity of the deposits in Jacob's Cavern. *Anthropol. Pap. Am. Mus.* **29**, 293–335.

Baker A., Smart P. L., Edwards R. L. and Richards D. A. (1993) Annual growth banding in a cave stalagmite. *Nature* **364**, 518–520.

Baker A., Smith C. L., Jex C., Fairchild I. J., Genty D. and Fuller L. (2008) Annually Laminated Speleothems: a review. *Int. J. Speleol.* **37**, 193–206.

Banner J. L. (1995) Application of the isotope and trace element geochemistry of strontium to studies of diagenesis in carbonate systems. *Sedimentology* **42**, 805–824.

Banner J. L., Guilfoyle A., James E. W., Stern L. A. and Musgrove M. (2007) Seasonal variation in modern speleothem calcite growth in central Texas, USA. *J. Sediment. Res.* **77**, 615–622.

Baskaran M. and Iliffe T. M. (1993) Age determination of recent cave deposits using excess ^{210}Pb – a new technique. *Geophys. Res. Lett.* **20**, 603–606.

Bajo P., Hellstrom J., Frisia S., Drysdale R., Black J., Woodhead J., Borsato A., Zanchetta G., Wallace M. W. and Regattieri E. (2016) "Cryptic" diagenesis and its implications for speleothem geochronologies. *Quaternary Sci. Rev.* **148**, 17–28.

Banks E. D., Taylor N. M., Gulley J., Lubbers B. R., Giarrizzo J. G., Bullen H. A., Hoehler T. M. and Barton H. A. (2010) Bacterial calcium carbonate precipitation in cave environments: a function of calcium homeostasis. *Geomicrobiol. J.* **27**(5), 444–454.

Belli R., Borsato A., Frisia S., Drysdale R., Maas R. and Greig A. (2017) Investigating the hydrological significance of stalagmite geochemistry (Mg, Sr) using Sr isotope and particulate element records across the Late Glacial-to-Holocene transition. *Geochim. Cosmochim. Acta* **199**, 247–263.

Boch R., Spötl C. and Frisia S. (2011) Origin and palaeoenvironmental significance of lamination in stalagmites from Katerloch Cave, Austria. *Sedimentology* **58**, 508–531.

Borsato A., Frisia S., Fairchild I. J., Somogyi A. and Susini J. (2007) Trace element distribution in annual stalagmite laminae mapped by micrometer-resolution X-ray fluorescence: implications for incorporation of environmentally significant species. *Geochim. Cosmochim. Acta* **71**, 1494–1512.

Caddeo G. A., Railsback L. B., De Waele J. and Frau F. (2015) Stable isotope data as constraints on models for the origin of coralloid and massive speleothems: the interplay of substrate, water supply, degassing, and evaporation. *Sediment. Geol.* **318**, 130–141.

Casteel R. C. and Banner J. L. (2015) Temperature-driven seasonal calcite growth and drip water trace element variations in a well-ventilated Texas cave: implications for speleothem paleoclimate studies. *Chem. Geol.* **392**, 43–58.

Couchoud I., Genty D., Hoffmann D., Drysdale R. and Blamart D. (2009) Millennial-scale climate variability during the Last Interglacial recorded in a speleothem from south-western France. *Quaternary Sci. Rev.* **28**, 3263–3274.

Cowan B. D., Osborn M. C. and Banner J. L. (2013) Temporal variability of cave-air CO_2 in central Texas. *J. Cave Karst Stud.* **75**, 38–50.

Cruz, Jr., F. W., Burns S. J., Jercinovic M., Karmann I., Sharp W. D. and Vuille M. (2007) Evidence of rainfall variations in Southern Brazil from trace element ratios (Mg/Ca and Sr/Ca) in a Late Pleistocene stalagmite. *Geochim. Cosmochim. Acta* **71**, 2250–2263.

Davies W. E. (1953) Geology of Pennsylvania caves. *Nat. Speleo. Soc. Bull.* **15**, 3–9.

Demény A., Czuppon G., Kern Z., Leél-Őssy S., Németh A., Szabó M., Tóth M., Wu C.-C., Shen C.-C. and Molnár M. (2016) Recrystallization-induced oxygen isotope changes in inclusion-hosted water of speleothems–Paleoclimatological implications. *Quatern. Int.* **415**, 25–32.

Dong J., Wang Y., Cheng H., Hardt B., Edwards R. L., Kong X., Wu J., Chen S., Liu D., Jiang X. and Zhao K. (2010) A high-resolution stalagmite record of the Holocene East Asian monsoon from Mt Shennongjia, central China. *Holocene* **20**, 257–264.

Dorale J. A., Edwards R. L., Alexander, Jr., E. C., Shen C. C., Richards D. A. and Cheng H. (2004) Uranium-series dating of speleothems: current techniques, limits, & applications. In *Studies of Cave Sediments*. Springer, US, pp. 177–197.

Fairchild I. J., Borsato A., Tooth A. F., Frisia S., Hawkesworth C. J., Huang Y.-M., McDermott F. and Spiro B. (2000) Controls on trace element (Sr-Mg) compositions of carbonate cave waters: implications for speleothem climatic records. *Chem. Geol.* **166**, 255–269.

Fairchild I. J., Baker A., Borsato A., Frisia S., Hinton R. W., McDermott F. and Tooth A. F. (2001) High-resolution, multiple-trace-element variation in speleothems. *J. Geol. Soc. Lon.* **158**, 831–841.

Fairchild I. J. and Treble P. C. (2009) Trace elements in speleothems as recorders of environmental change. *Quaternary Sci. Rev.* **28**, 449–468.

Feng W., Banner J. L., Guilfoyle A., Musgrove M. and James E. W. (2012) Oxygen isotopic fractionation between drip water and speleothem calcite: a 10-year monitoring study, central Texas, USA. *Chem. Geol.* **304–305**, 53–67.

Feng W., Casteel R. C., Banner J. L. and Heinze-Fry A. (2014) Oxygen isotope variations in rainfall, drip-water and speleothem calcite from a well-ventilated cave in Texas, USA: assessing a new speleothem temperature proxy. *Geochim. Cosmochim. Acta* **127**, 233–250.

Frisia S., Borsato A., Fairchild I. J. and McDermott F. (2000) Calcite fabrics, growth mechanisms and environments of formation in speleothems (Italian Alps and SW Ireland). *J. Sediment. Res.* **70**, 1183–1196.

Gascoyne M. (1992) Palaeoclimate determination from cave calcite deposits. *Quat. Sci. Rev.* **11**, 609–632.

Genty D. (1992) Les spéléothèmes du tunnel de Godarville (Belgique)—un exemple exceptionnel de concrétionnement moderne—intérêt pour l'étude de la cinétique de la précipitation de la calcite etde sa relation avec les variations d'environnement. *Speleochronos* **4**, 3–29.

Genty D. (1993) Mise en évidence d'alternances saisonnières dans la structure interne des stalagmites. Intérêt pour la reconstitution des paléoenvironnements continentaux. *C. R. Acad. Sci. Paris* **317**(2), 1229–1236.

Genty D. and Quinif Y. (1996) Annually laminated sequences in the internal structure of some Belgian stalagmites –importance for Paleoclimatology. *J. Sediment. Res.* **66**, 275–288.

Genty D., Baker A. and Barnes W. (1997) Comparaison entre les lamines luminescentes et les lamines visibles annuelles de stalagmites. *C. R. Acad. Sci. Paris* **325**, 193–200.

Genty D., Vokal B., Obelic B. and Massault M. (1998) Bomb 14C time history recorded in two modern stalagmites – importance for soil organic matter dynamics and bomb 14C distribution over continents. *Earth Planet. Sci. Lett.* **160**, 795–809.

Genty D., Massault M., Gilmour M., Baker A., Verheyden S. and Keppens E. (1999) Calculation of past dead carbon proportion and variability by the comparisonof AMS ^{14}C and TIMS U/Th ages on two Holocene stalagmites. *Radiocarbon* **41**(3), 251–270.

Genty D., Baker A., Massault M., Procror Ch., Gilmour M., Pons-Branchu E. and Hamelin B. (2001a) Dead carbon in stalagmites: limestone paleodissolution versus ageing of soil organic matter – implications for 13c variations in stalagmites. *Geochim. Cosmochim. Acta* **65**, 3443–3457.

Genty D., Baker A. and Vokal B. (2001b) Intra- and inter-annual growth rate of modern stalagmites. *Chem. Geol.* **176**(1–4), 191–212.

Goede A., Veeh H. H. and Ayliffe L. K. (1990) Late quaternary palaeotemperature records for two Tasmanian speleothems. *Aust. J. Earth Sci.* **37**, 267–278.

Hendy C. H. (1971) The isotopic geochemistry of speleothems—I. The calculation of the effects of different modes of formation on the isotopic composition of speleothems and their applicability as palaeoclimate indicators. *Geochim. Cosmochim. Acta* **35**, 801–824.

Hodge E., McDonald J., Fischer M., Redwood D., Hua Q., Levchenko V., Drysdale R., Waring C. and Fink D. (2011) Using the ^{14}C bomb pulse to date young speleothems. *Radiocarbon* **53**, 345–357.

Hua Q., McDonald J., Redwood D., Drysdale R., Lee S., Fallon S. and Hellstrom J. (2012) Robust chronological reconstruction for young speleothems using radiocarbon. *Quat. Geochronol.* **14**, 67–80.

Hua Q., Barbetti M. and Rakowski A. (2013) Atmospheric radiocarbon for the period 1950–2010. *Radiocarbon* **55**, 2059–2072.

Huang Y.-M. and Fairchild I. J. (2001) Partitioning of Sr^{2+} and Mg^{2+} into calcite under karst-analogue experimental conditions. *Geochim. Cosmochim. Acta* **65**, 47–62.

Huang Y., Fairchild I. J., Borsato A., Frisia S., Cassidy N. J., McDermott F. and Hawkesworth C. J. (2001) Seasonal variations in Sr, Mg and P in modern speleothems (Grotta di Ernesto, Italy). *Chem. Geol.* **175**, 429–448.

James E. W., Banner J. L. and Hardt B. (2015) A global model for cave ventilation and seasonal bias in speleothem climate records. *Geochem. Geophy. Geosy.* **16**, 1044–1051.

Johnson K. R., Hu C., Belshaw N. S. and Henderson G. M. (2006) Seasonal trace-element and stable-isotope variations in a Chinese speleothem: the potential for high-resolution paleomonsoon reconstruction. *Earth Planet. Sc. Lett.* **244**, 394–407.

Kim S. T. and O'Neil J. R. (1997) Equilibrium and nonequilibrium oxygen isotope effects in synthetic carbonates. *Geochim. Cosmochim. Acta* **61**, 3461–3475.

Košler J. (2008) Laser ablation sampling stratigies for concentration nd isotope ratio analyses by ICP-MS. *Laser Ablation ICP-MS Earth Sci.: Curr. Pract. Outstanding Iss.* **40**, 79–92.

Kuczumow A., Genty D., Chevallier P., Nowak J. and Ro C.-U. (2003) Annual resolution analysis of a SW-France stalagmite by X-ray synchrotron microprobe analysis. *Spectrochim. Acta Part B: Atom. Spectrosc.* **58**(5), 851–865.

Larkin D. A. and Bomar G. W. (1983) *Climatic Atlas of Texas*. Texas Department of Water Resources, Austin, TX.

Lauritzen S.-E. and Lundberg J. (1999) Speleothems and climate: a special issue of The Holocene. *Holocene* **9**, 643–647.

Levin I., Kromer B., Schoch-Fischer H., Bruns M., Münnich M., Berdau D., Vogel J. C., Münnich K. O. (1994). Δ14CO2 records from two sites in central Europe. In Trends 93—A Compendium of Data on Global Change and online updates (eds. T. A. Boden, D. P. Kaiser, R. J. Sepanski, F. W. Stoss). Oak Ridge, Tennessee, USA: Carbon Dioxide Information Analysis Center, Oak Ridge National Laboratory. pp. 203–222.

Lorens R. B. (1981) Sr, Cd, Mn and Co distribution coefficients in calcite as a function of calcite precipitation rate. *Geochim. Cosmochim. Acta* **45**, 553–561.

Mattey D., Lowry D., Duffet J., Fisher R., Hodge E. and Frisia S. (2008) A 53 year seasonally resolved oxygen and carbon isotope record from a modern Gibraltar speleothem: reconstructed drip water and relationship to local precipitation. *Earth Planet. Sc. Lett.* **269**, 80–95.

Mattey D. P., Fairchild I. J., Atkinson T. C., Latin J.-P., Ainsworth M. and Durell R. (2010) Seasonal microclimate control of calcite fabrics, stable isotopes and trace elements in modern speleothem from St Michaels Cave, Gibraltar. *Geol. Soc. Lond. Sp.* **336**, 323–344.

McCrea J. M. (1950) On the isotopic chemistry of carbonates and a paleotemperature scale. *J. Chem. Phys.* **18**, 849–857.

McDermott F. (2004) Palaeo-climate reconstruction from stable isotope variations in speleothems: a review. *Quat. Sci. Rev.* **23**, 901–918.

McGarry S. F. and Baker A. (2000) Organic acid fluorescence: applications to speleothem palaeoenvironmental reconstruction. *Quaternary Sci. Rev.* **19**, 1087–1101.

Mucci A. (1987) Influence of temperature on the composition of magnesian calcite overgrowths precipitated from seawater. *Geochim. Cosmochim. Acta* **51**, l977–1984.

Mucci A. and Morse J. W. (1983) The incorporation of Mg+2 and Sr+2 into calcite overgrowths: influences of growth rate and solution composition. *Geochim. Cosmochim. Acta* **47**, 217–233.

Musgrove M. and Banner J. L. (2004) Controls on the spatial and temporal variability of vadose dripwater geochemistry: Edwards Aquifer, central Texas. *Geochim. Cosmochim. Acta* **68**, 1007–1020.

Nagra G., Treble P. C., Andersen M. S., Bajo P., Hellstrom J. and Baker A. (2017) Dating stalagmites in Mediterranean climates using annual trace element cycles. *Sci. Rep.* **7**, 621.

Nielsen-Gammon J. W. (2012) The 2011 Texas Drought. *Texas Water J.* **3**, 59–95.

Noronha A. L., Johnson K. R., Southon J. R., Hu C., Ruan J. and McCabe-Glynn S. (2015) Radiocarbon evidence for decomposition of aged organic matter in the vadose zone as the main source of speleothem carbon. *Quaternary Sci. Rev.* **127**, 37–47.

Orland I. J., Burstyn Y., Bar-Matthews M., Kozdon R., Ayalon A., Matthews A. and Valley J. W. (2014) Seasonal climate signals (1990–2008) in a modern Soreq Cave stalagmite as revealed by high-resolution geochemical analysis. *Chem. Geol.* **383**, 322–333.

Orland I. J., Edwards R. L., Cheng H., Kozdon R., Cross M. and Valley J. W. (2015) Direct measurements of deglacial monsoon strength in a Chinese stalagmite. *Geology* **43**, 555–558.

Raich J. W., Potter C. S. and Bhagawati D. (2002) Interannual variability in global soil respiration, 1980–94. *Glob. Change Biol.* **8**, 800–812.

Railsback L. B., Brook G. A., Chen J., Kalin R. and Fleisher C. J. (1994) Environmental controls on the petrology of a late Holocene speleothem from Botswana with annual layers of aragonite and calcite. *J. Sediment. Res.* **64**, 147–155.

Reddell A. R. and Smith J. (1962) Brunton and tape survey: Hammett's Cave, Travis County, Texas. Texas Speleological Survey, Modified 1973 by R. Fieseler. Available from <www.utexas.edu/tmm/sponsered_sites/tss/CaveMaps/index.html>.

Roberts M. S., Smart P. L. and Baker A. (1998) Annual trace element variations in a Holocene speleothem. *Earth Planet. Sc. Lett.* **154**, 237–246.

Rosenthal Y., Boyle E. A. and Slowey N. (1997) Temperature control on the incorporation of Mg, Sr, F, and Cd into benthic foraminiferal shells from Little Bahama Bank: prospects for thermocline paleoceanography. *Geochim. Cosmochim. Acta* **61** (17), 3633–3643.

Rupper S., Roe G. and Gillespie A. (2009) Spatial patterns of Holocene glacier advance and retreat in Central Asia. *Quaternary Res.* **72**, 337–346.

Rutlidge H., Baker A., Marjo C. E., Andersen M. S., Graham P. W., Cuthbert M. O., Rau G. C., Roshan H., Markowska M., Mariethoz G. and Jex C. N. (2014) Dripwater organic matter and trace element geochemistry in a semi-arid karst environment: implications for speleothem paleoclimatology. *Geochim. Cosmochim. Acta* **135**, 217–230.

Schwarcz H. P. (1986) Geochronology and isotopic geochemistry of speleothems. In Handbook of Environmental Isotope Geochemistry. The Terrestrial Environment B, vol. 2 (eds. P. Fritz, G. Fontes). Amsterdam, Elsevier. pp. 271–303.

Schwartz M., Ahas R. and Aasa A. (2006) Onset of spring starting earlier across the Northern Hemisphere. *Glob. Change Biol.* **12**, 343–351.

Shen, C., Lin, K. Duan, W., Jiang, X., Partin, J. W., Edwards, R. L., Cheng, H. and Tan, M. (2013) Testing the annual nature of banding. Sci. Rep. 3 (Article number: 2633).

Shopov Y. Y., Ford D. C. and Schwarcz H. P. (1994) Luminescent microbanding in speleothems: high-resolution chronology and paleoclimate. *Geology* **22**, 407–410.

Sinclair D. J., Banner J. L., Taylor F. W., Partin J., Jenson J., Mylroie J., Goddard E., Quinn T., Jocson J. and Miklavič B. (2012) Magnesium and strontium systematics in tropical speleothems from the Western Pacific. *Chem. Geol.* **294–295**, 1–17.

Smith C. L., Fairchild I. J., Spötl C., Frisia S., Borsato A., Moreton S. G. and Wyn P. M. (2009) Chronology building using objective identification of annual signals in trace element profiles of stalagmites. *Quat. Geochron.* **4**, 11–21.

Spötl C., Fairchild I. J. and Tooth A. F. (2005) Cave air control on dripwater geochemistry, Obir Caves (Austria): implications for speleothem deposition in dynamically ventilated caves. *Geochim. Cosmochim. Acta* **69**, 2451–2468.

Stevanović Z. (2018) Global distribution and use of water from karst aquifers. In *Advances in Karst Research: Theory, Fieldwork and Applications Geol. Soc. Lond Sp* (eds. M. Parise, F. Gabrovsek, G. Kaufmann and N. Ravbar), p. 466.

Tan M., Baker A., Genty D., Smith C., Esper J. and Cai B. (2006) Applications of stalagmite laminae to paleoclimate reconstructions: comparison with dendrochronology/climatology. *Quaternary Sci. Rev.* **25**, 2103–2117.

Tesoriero A. J. and Pankow J. F. (1996) Solid solution partitioning of Sr^{2+}, Ba^{2+} and Cd^{2+} into calcite. *Geochim. Cosmochim. Acta* **60**, 1053–1063.

Treble P., Shelley J. M. G. and Chappell J. (2003) Comparison of high resolution sub-annual records of trace elements in a modern (1911–1992) speleothem with instrumental climate data from southwest Australia. *Earth Planet. Sci. Lett.* **216**, 141–153.

Treble P. C., Chappell J., Gagan M. K., McKeegan K. D. and Harrison T. M. (2005) In situ measurement of seasonal $\delta^{18}O$ variations and analysis of isotopic trends in a modern speleothem from southwest Australia. *Earth Planet. Sci. Lett.* **233**, 17–32.

Tremaine D. M., Froelich P. N. and Wang Y. (2011) Speleothem calcite farmed *in situ*: Modern calibration of $\delta^{18}O$ and $\delta^{13}C$ paleoclimate proxies in a continuously-monitored natural cave system. *Geochim. Cosmochim. Acta* **75**, 4929–4950.

Wang Y. J., Cheng H., Edwards R. L., An Z. S., Wu J. Y., Shen C.-C. and Dorale J. A. (2001) A high-resolution absolute-dated late pleistocene monsoon record from Hulu Cave, China. *Science* **294**, 2345–2348.

Weiss J. L., Castro C. L. and Overpeck J. T. (2009) Distinguishing pronounced droughts in the southwestern United States: seasonality and effects of warmer temperatures. *J. Clim.* **22**, 5918–5932.

White W. B. (2007) Cave sediments and paleoclimate. *J. Cave Karst Stud.* **69**, 76–93.

Wolter K., Dole R. M. and Smith C. A. (1999) Short-term climate extremes over the continental United States and ENSO. Part I: Seasonal temperatures. *J. Clim.* **12**, 3255–3272.

Wong C. I., Banner J. L. and Musgrove M. (2011) Seasonal dripwater Mg/Ca and Sr/Ca variations driven by cave ventilation: Implications for and modeling of speleothem paleoclimate records. *Geochim. Cosmochim. Acta* **75**, 3514–3529.

Associate editor: Miryam Bar-Matthews